



HAL
open science

Characterization and modelling of looming-sensitive neurons in the crab *Neohelice*

Julia Carbone, Agustín Gabriel Yabo, Damian Oliva

► **To cite this version:**

Julia Carbone, Agustín Gabriel Yabo, Damian Oliva. Characterization and modelling of looming-sensitive neurons in the crab *Neohelice*. *Journal of Comparative Physiology A*, 2018, 204 (5), pp.487-503. 10.1007/s00359-018-1257-1 . hal-03928580

HAL Id: hal-03928580

<https://hal.science/hal-03928580>

Submitted on 7 Jan 2023

HAL is a multi-disciplinary open access archive for the deposit and dissemination of scientific research documents, whether they are published or not. The documents may come from teaching and research institutions in France or abroad, or from public or private research centers.

L'archive ouverte pluridisciplinaire **HAL**, est destinée au dépôt et à la diffusion de documents scientifiques de niveau recherche, publiés ou non, émanant des établissements d'enseignement et de recherche français ou étrangers, des laboratoires publics ou privés.

1
2
3
4 **Characterization and modelling of Looming-Sensitive Neurons in the crab**
5 ***Neohelice***
6

7
8 Julia Carbone¹, Agustín Yabo¹, and Damian Oliva¹
9

10
11 ¹ Departamento de Ciencia y Tecnología, Universidad Nacional de Quilmes. Roque S. Peña 352,
12
13 (1876) Bernal, Pcia de Buenos Aires, Argentina.
14
15

16
17 **e-mail:** doliva@unq.edu.ar
18
19

20
21 **SUMMARY**
22

23 Looming-sensitive neurons (LSNs) are motion-sensitive neurons tuned for detecting imminent collision.
24 Their main characteristic is the selectivity to looming (a 2D representation of an object approach), rather than to
25 receding, stimuli. In this work, we studied a set of LSNs by performing surface extracellular recordings in the
26 optic nerve of *Neohelice granulata* crabs, and characterized their response against a wide range of computer-
27 generated visual stimuli with different combinations of moving edges, highlighting different components of the
28 optical flow. In addition to their selectivity to looming stimuli, we characterized other properties of these
29 neurons, such as low directionality; reduced response to sustained excitement; and an inhibition phenomena in
30 response to visual stimuli with dense optical flow of expansion, contraction, and translation. To analyze the
31 spatio-temporal processing of these LSNs, we proposed a biologically plausible computational model which was
32 inspired by previous computational models of the locust LGMD neuron. The videos seen by the animal during
33 electrophysiological experiments were applied as an input to the model which produced a satisfactory fit to the
34 measured responses, suggesting that the computation performed by LSNs in a decapod crustacean appears to be
35 based on similar physiological processing previously described for the LGMD in insects.
36
37
38
39
40
41
42
43
44
45
46
47
48

49 **KEYWORDS:** *motion detection; collision avoidance; looming; crustacean; vision*
50
51
52
53
54
55
56
57
58
59
60
61
62
63
64
65

1
2
3
4 **INTRODUCTION**
5
6
7

8 Arthropods (especially insects and crustaceans) are important animal models for studying the
9 neurophysiological bases of visual processing and visually guided behaviors. This is primarily due to
10 the variety and complexity of the behaviors they exhibit, together with the relative simplicity of their
11 nervous systems (Srinivasan and Zhang 2004; Hemmi and Tomsic 2012). The performance of these
12 visuomotor behaviors strongly depends, at the sensory level, on a set of Motion-Sensitive Neurons
13 (MSNs), which can perform specialized spatio-temporal processing and integration of the information
14 relating to the optical flow (OF) field. The OF is defined as the apparent motion of the image intensities
15 (or brightness patterns), and ideally corresponds to the velocity field: the 2D projection onto a retina of
16 the relative 3D motion of scene points (Nelson and Aloimonos 1988). Using the information extracted
17 from the OF (adapted to the nature of the task and the environmental conditions), an animal can
18 analyze the motion of predators, prey or conspecifics, and can also extract information about its own
19 movement relative to fixed objects.
20
21
22
23
24
25
26
27
28
29

30 In relation to insects, a paradigmatic example of MSNs are the lobula plate neurons (LPNs) of
31 the fly, which act as neuronal matched filters producing an accurate and continuous report of the
32 overall state of wide-field optical flow generated by its self-motion (Krapp and Hengstenberg 1996).
33 This is achieved through a nonlinear spatio-temporal integration of information from elementary
34 motion detectors that locally encode the direction of the OF field. Another paradigmatic example of a
35 motion detector in insects is the lobula giant motion detector (LGMD) neuron (Rind and Simmons
36 1999), which has been proposed as an important element in avoidance behaviors to imminent collision
37 (Fotowat and Gabbiani 2011). Its main characteristic is the tuning to looming, rather than to receding,
38 stimuli. This property manifests in a selectivity to the stimuli on a collision trajectory, since although
39 the looming and receding stimuli activate the same photoreceptors with the same angular speed (but
40 with reversed direction), the LGMD neuron produces a much greater response to expansion than
41 contraction. In the last years, diverse MSNs have been characterized in different species, exhibiting a
42 similar processing as that of the LGMD, and were jointly denominated as Looming-Sensitive Neurons
43 (LSNs). Examples of insects LSNs have been characterized in locusts (Rind and Simmons 1992,
44 Gabbiani et al. 1999, Gray et al. 2010, Rosner and Homberg 2013), flies (Borst 1991), and praying
45 mantis (Yamawaki 2009); and in vertebrates, LSNs were found in pigeons (Wang and Frost, 1992) and
46 fish (Preuss et al. 2006, Dunn et al. 2016).
47
48
49
50
51
52
53
54
55
56
57
58
59
60
61
62
63
64
65

1
2
3
4 In crustaceans, the existence of MSNs (known as jittery motion detectors) with sensitivity to
5 looming stimuli has been reported in lobsters (Glantz 1974). In the crab *Neohelice granulata*, four
6 neuronal types of MSNs were identified in the lobula (third optic neuropil), and two monostratified
7 lobula giant neurons (MLGs) show typical characteristics of LSNs (Oliva et al. 2017; Medan et al.
8 2007; Tomsic et al. 2017).
9

10
11
12
13 Neuroanatomical studies indicate that the visual nervous systems of insects and decapod
14 crustaceans may be homologous (Strausfeld 2005). Nilsson and Osorio (1998) proposed important
15 evidence supporting this hypothesis, including that insects and malacostracan crustaceans have: a)
16 nearly identical compound eyes sharing the same cellular composition of the ommatidia, b) the same
17 general layout of the optic ganglia, and c) important similarities of structural and physiological neuron
18 types in the first optic ganglion. At the level of the lobula, MSNs are also elements common to insects
19 and crustaceans, with large tangential processes collecting information from extensive parts of the
20 retinotopic mosaic and with axons projecting to the midbrain (e.g., Sztarker et al. 2005; Medan et al.
21 2007).
22
23
24
25
26
27
28
29

30 Given this proposed homology in their visual system morphology, it is interesting to compare
31 the looming stimuli processing in LSN neurons of insects and a decapod crustacean. To accomplish
32 this, in the first part of this work, we characterized the visual response in a set of MSNs by extracellular
33 recordings in the optic nerve of *N. granulata* crabs (also referred to in this publication as *Neohelice*).
34 Using this technique, we characterized the neuronal response against a wide range of optical flow
35 patterns, showing that the measured MSNs were highly sensitive to looming stimuli, and therefore can
36 be classified as LSNs. In the second part of the study, we proposed a biologically plausible
37 computational model based on previous experimental results and computational models of the insect
38 LGMD neuron. We started from a previously proposed model for *Neohelice*'s MLG neurons (Oliva
39 and Tomsic 2014) and we incorporated two improvements to that model that allowed us to simulate the
40 neuronal response to the wide set of stimuli applied in this work: the model's inputs were the videos
41 observed by the animal during the electrophysiological experiments, and we incorporated the
42 phenomenon of presynaptic lateral inhibition previously modeled in the LGMD (Rind and Bramwell
43 1996, Rind et al. 2016). The model helped us analyze the spatio-temporal processing for the LSNs
44 measured in this work showing that the computation performed by LSNs in a decapod crustacean
45 appears to be based on similar physiological processing previously described for the LGMD in insects.
46
47
48
49
50
51
52
53
54
55
56
57
58
59
60
61
62
63
64
65

METHODS

Animals

Animals used were adult male *Neohelice* (previously *Chasmagnathus*) *granulata* crabs measuring 2.7–3.0 cm across the carapace and weighing approximately 17 g. The crabs were collected in the rías (narrow coastal inlets) of San Clemente del Tuyú, Argentina, and transported to the laboratory, where they were housed in plastic tanks (35 × 48 × 27 cm) that were filled to a depth of 2 cm with diluted seawater, to a density of 20 crabs per tank. The water used in the tanks and other containers during the experiments was prepared using hw-Marinex (Winex, Hamburg, Germany), at a salinity of 10–14‰, pH 7.4–7.6, and maintained within a temperature range of 22–24°C. The holding and experimental rooms were maintained on a 12 h:12 h light:dark cycle (lights on from 07:00 to 19:00 h), and the experiments were performed between 08:00 and 19:00 h. Crabs were fed rabbit pellets (Nutrients, Buenos Aires, Argentina) every three days, and the water was changed after feeding.

Visual stimuli

Computer-generated visual stimuli were projected on a flat-screen monitor (LG 18.5”); horizontal and vertical screen dimensions were 41 cm by 23 cm, respectively, refreshing rate 60 Hz). Irradiance on the monitor screen was 4 mW/m² (black) and 205 mW/m² (white background).

Changes in luminance: These stimuli simulate the instantaneous appearance of dark objects. The sizes of the objects tested were: 0.5°, 1.9°, 3.9°, 7.3°, and 14.5°.

Moving stimuli that highlighted different components of OF: The OF field seen by an animal can be split into two components: rotational and translational (Nelson and Aloimonos 1988). The following set of visual stimuli was designed to emphasize these two components (see Fig. 1).

A) *Moving edges at constant angular velocity:* A relative turning about a fixed axis, between the animal and the objects, results in a rotational optical flow field (ROF). The ROF was produced by moving a dark edge in three different directions (denoted as ME(1-3)) over a white background with a constant angular velocity of $\theta' = 26$ °/s (Fig. 1a). Since there is only a single edge moving on the screen, the ME(1-3) stimuli produced a sparse ROF. In order to detect the possible presence of lateral inhibition phenomena, we also stimulated with an optomotor pattern (denoted as OPTO), moving at

1
2
3
4 constant angular velocity ($\theta' = 26^\circ/\text{s}$, $\Delta\phi = 12^\circ$), (Fig. 1a). This stimulus simulated the movement of
5 many objects when the animal rotates around its own vertical axis and generated a dense ROF.
6
7
8

9
10 **B) Looming and receding:** A relative approach between the animal and an object produces a
11 translational optical flow (TOF) with an expansion in the direction of motion. The TOF of expansion
12 was generated with looming stimuli (denoted as LOOM) which are simulated by dark squares of
13 various sizes approaching at constant speeds on a direct collision course towards the animal (Fig. 1b).
14
15

16 Because a single object approaching on a white background was simulated, these stimuli
17 produced a sparse TOF of expansion. The stimuli applied has been described in detail elsewhere (Oliva
18 et al. 2007; Oliva and Tomsic 2014). Briefly, l denotes the object half-size. The distance between the
19 animal eye and virtual object at time t is $x(t) = L - v \cdot t$, and the object subtends an angle $\theta(t)$ on the eye.
20
21 Thus, we can write:
22
23
24

$$\tan(\theta/2) = \frac{l}{L - v \cdot t} = \frac{1}{L/l - v \cdot t/l} = \frac{1}{1/\tan(\theta_0/2) - t/(l/v)} \quad \text{Eq.1}$$

25
26
27
28
29

30 With the chosen coordinate system and time definitions, we have $x(t) \geq 0$, $t \geq 0$. Where v is the
31 absolute value of the approach speed. Eq. 1 indicates that each stimulus is characterized by a value of
32 l/v and of θ_0 . Objects were simulated to start their approach from a distance L of 5 m. Due to the limits
33 imposed by the screen's size and distance from the animal's eye, the maximum stimulus expansion was
34 $\theta = 60^\circ$. We used a total of six looming stimuli (Table 1). In addition to the looming stimulus, we also
35 simulated a receding stimulus (denoted as RECED) which represented the object moving away at speed
36 v . This stimulus presented the same angular size values as the looming stimulus, but with an inverted
37 temporal sequence (Table 1, stimulus 2). Under these conditions, the receding stimulus generated a
38 sparse TOF of contraction.
39
40
41
42
43
44
45
46
47
48

49 **C) Looming and receding patterns:** These stimuli simulated a situation in which the animal runs while
50 observing many fixed objects in the environment (Fig. 1c). We simulated the animal traveling at a
51 speed $v = 17 \text{ cm/s}$, within a quadrangular tube of height $H = 2 \cdot l = 4 \text{ cm}$, therefore the stimulus
52 produced a sequence of superimposed looming stimuli with an $l/v = 0.117 \text{ s}$ (similar to the value of
53 stimulus 2 in Table 1). Looming and receding patterns correspond to a dense TOF of expansion and
54 contraction and are denoted LOOM-P and RECED-P, respectively. The simulation was generated by
55 the superposition of loomings or recedings; in which LOOM-P corresponds to the visual stimulus
56
57
58
59
60
61
62
63
64
65

1
2
3
4 observed in the direction of movement and RECED-P to the visual stimuli observed in the opposite
5 direction to the movement. It is important to note that the edge pattern was repeated with a spatial
6 period $\lambda = 17$ cm; therefore, the temporal frequency of the passage of the edges was: $f = v/\lambda = 1$ Hz.
7
8
9

10 11 *Electrophysiology*

12
13 For dissection, the crab was sedated in a container (bowl) with ice and its chelae fixed with
14 acrylic glue. The crab was positioned in the center of the arrangement of monitors within the Faraday
15 cage. The clamp with the crab was held in position using a magnetic holding device (Fig. 2a). The
16 eyestalks were immobilized with a piece of paper, maintaining the view at an angle of $40^\circ \pm 10$ with
17 the screen. Next, the animal's statocyte was removed under a magnifying glass and the optic nerve was
18 found (which corresponds to the Protocerebral tract in Medan et al (2007)). Once the nerve was
19 reached, it was contacted with a suction electrode (borosilicate glass; 1.2 mm outer diameter, 0.68 mm
20 inner diameter) pulled with a Brown-Flaming micropipette puller (P-97; Sutter Instrument, Novato,
21 CA, USA). Electrode resistance was approximately 40 K Ω . The suction electrode was positioned with
22 a micromanipulator NARISHIGE (Japan). The electrode's signal steadily remained around 30 μ V
23 during the stimulation and the signal was amplified and digitized with the RHA2000 (Intantech)
24 system. Two computers were used: PC1 was used to visually stimulate the crab by projecting images
25 generated on the monitor with a frequency of 60 Hz (Psychtoolbox - Matlab, The MathWorks, Inc.,
26 Natick, MA, USA). PC2 recorded the electrophysiological activity through an Intan Amplifier software
27 at a sampling frequency of 25 kHz. Finally, PC1 was connected to PC2 via an auxiliary wire, which
28 allowed synchronization of the recordings.
29
30
31
32
33
34
35
36
37
38
39
40
41
42

43 Similar to methods used in a previous work (Oliva et al. 2007), we began stimulation after the
44 animal had remained visually undisturbed for 3 min inside the setup, and the inter-trial interval was set
45 to 1 min to minimize the effect of habituation on the neuronal response. A total of 15 neurons from 9
46 animals were studied. Only one neuron showed a directional response and was separated from the 14
47 non-directional neurons that were studied in this work. In the first phase of the experiment, the intensity
48 of the neuronal response was measured by applying a looming stimulus (stimulus 2 from Table 1)
49 alternately on three positions around the animal (Fig. 2a, right panel). The firing rate was maximal
50 upon stimulation in the ipsilateral monitor (right screen), for this reason, the characterization of the
51 neuronal processing for the wide set of stimuli was performed using this monitor (more details in
52 Results section).
53
54
55
56
57
58
59
60
61
62
63
64
65

1
2
3
4 During the experiment, crabs intermittently moved their legs for a few seconds, but generally these
5 movements did not affect the electrode seal. The technique of extracellular measurement with suction
6 electrodes allowed prolonged recording lasting between 3 and 5 hours.
7
8
9

10 11 **Data analysis**

12 The spike sorting process consisted of the following steps (Quiari Quiroga 2007): a) the
13 continuous raw data was band-pass filtered between 300 Hz and 3000 Hz; b) the spikes were detected
14 using an amplitude threshold (Thr) set to $Thr = 5\sigma_n$, where σ_n was an estimate of the standard deviation
15 of the bandpass filtered background noise, c) the relevant features of the spike shapes were extracted,
16 thus giving a dimensionality reduction, and finally d) the features were the input of a clustering
17 algorithm that performs the classification. In this work, two basic approaches of spike sorting were
18 tested. The first method applied was the WaveClus software (Quiroga et al. 2004; Wild et al. 2012). In
19 the second method, we selected a 1-ms wide window around each detected spike, generating a vector of
20 dimension (25×1). To extract the relevant characteristics of these vectors, the principal components
21 analysis (PCA) method (first 5 components) was used. In addition, a K-means algorithm was used for
22 clustering different neurons. The optimal number of clusters was determined according to the criteria of
23 Calinski-Harabasz and Davies-Bouldin. The two methods detected 1 to 3 spike classes for all
24 recordings (Fig. 2b-c). All data analysis procedures were written in Matlab (The MathWorks, Inc.,
25 Natick, MA, USA). Both methods produced similar spike sorting results. We estimated the
26 instantaneous firing rate by convolving the spike trains with a square window (width of 200 ms) and
27 normalizing the resulting waveform such that its integral was equal to the total number of spikes over
28 the entire trial (Gabbiani et al. 1999). The Kruskal–Wallis test was used to compare the medians of
29 samples across different stimuli (P-values were denoted as P_{KW}). To compare two groups, a sign test
30 was used (P-values were denoted as P_{SIGN}). The parameters of the different proposed models were
31 estimated by nonlinear least-squares error minimization (*nlinfit* and *patternsearch* algorithms in
32 Matlab). The uncertainties (standard deviation) of the model parameters were estimated using the
33 bootstrap method (Wasserman 2004). All data analysis procedures were written in Matlab (The
34 MathWorks, Inc., Natick, MA, USA).
35
36
37
38
39
40
41
42
43
44
45
46
47
48
49
50
51
52
53
54
55
56
57
58
59
60
61
62
63
64
65

RESULTS

Neuronal response to changes in luminance

Figure 3a shows the neuronal responses to a local luminance change associated with the appearance of a dark square of angular size θ . Similarly to what was described in previous work for lobula giant neurons (Beron de Astrada and Tomsic 2002), responses to changes in luminance were phasic. In all of the measured neurons, responses were not detected for the stimulus with an angular size of 0.5° and the intensity of the phasic response increased with the angular size of the visual area stimulated. Figure 3b shows the number of spikes emitted as a function of the angular size of the square. This curve was adjusted as $R(\theta) = \alpha \cdot (\theta - \beta)^\gamma$, (for $\theta > \beta$) where θ is the angular size of the square. The values obtained by least-squares were: units $\alpha = 1.94 \pm 0.8$, $\beta = 0.66^\circ \pm 0.57^\circ$, $\gamma = 0.85 \pm 0.15$. Interestingly, the value of the parameter β obtained by the fit was similar to estimates for ommatidial minimum size. In fact, in the lateral part of the eye, the interommatidial angles vary between 0.6° and 0.4° , respectively (Berón de Astrada et al. 2012).

Neuronal response to moving edges at constant angular velocity

Figure 4a shows a typical extracellular recording, a firing rate response from a typical neuron, and the average firing rate as a function of time in response to moving edges at constant angular velocity from 14 neurons from 9 different animals (one average response, per stimulus and per neuron were included in the analyses). The first three traces correspond to dark moving edges going through a white background in different directions ME (1-3), producing a sparse ROF. An initial phasic response was observed for the three stimuli. The fourth trace shows the response to OPTO stimulus (corresponding to a dense ROF), where we observed an initial intense response that abruptly decreased. Figure 4b shows the maximum firing rate for each stimuli; no significant differences were found when using this parameter to compare between the stimuli ($P_{KW} = 0.32$). However, we found significant differences between the mean firing rate during the stimulation (Fig. 4c). The stimulus OPTO produced a significantly lower response ($P_{KW} < 0.01$).

Finally, to analyze the directionality of the neuronal response, we performed comparisons between the three stimuli ME (1-3) for individual neurons. We studied a set of 9 neurons for which it was possible to record more than five trials for each stimulus, and compared (for each neuron separately) the mean firing rate during stimulation. In 8 neurons, no significant differences for the three

1
2
3
4 directions of movement were found and, therefore, we concluded that the measured neurons did not
5 present a significant degree of directionality in their response. The neuron that showed a directional
6 response was separated from the group of non-directional neurons and was not included in this
7 analysis.
8
9

10 11 12 13 14 15 ***The neuronal response to looming and receding***

16
17 Figure 5a shows the typical extracellular recordings, a firing rate response from a typical
18 neuron, and the average firing rate versus time for the stimuli LOOM, RECED, LOOM-P, and
19 RECED-P from 14 neurons from 9 different animals (one average response per stimulus and per
20 neuron were included in the analyses). These four stimuli produced sparse (or dense) optical flow of
21 expansion or contraction. Figure 5b shows the maximum firing rate produced by each stimulus. The
22 looming stimulus produced the highest maximum firing rate for all stimuli ($P_{KW} < 0.01$). The response
23 to LOOM was significantly higher than the response to RECED ($P_{SIGN} < 0.05$). Similarly, LOOM-P
24 and RECED-P were compared and significant differences were detected in favor of stimulus LOOM-P
25 ($P_{SIGN} < 0.05$). Finally, LOOM and LOOM-P were also compared and significant differences were
26 detected in favor of stimulus LOOM ($P_{SIGN} < 0.05$). In summary, the measured MSNs were highly
27 sensitive to looming stimuli (sparse and dense TOF of expansion), and therefore can be classified as
28 LSNs.
29
30
31
32
33
34
35
36
37
38
39
40

41 ***LSN response to looming stimuli from different approaching directions***

42
43 To study the sensitivity of the LSNs to looming stimuli from different approaching directions,
44 the neuronal response was recorded by applying a looming stimulus (stimulus 2 from Table 1)
45 alternately on the three screens around the animal (Fig. 2a, right panel). Figure 6a shows a typical
46 peristimulus time histogram for one of the neurons detected in Fig. 2c. To quantify the intensity of the
47 response to the stimulation from each screen, the standardized response r was defined as $r(n) = R_{max}$
48 $(n)/R_{max}(R)$, where $n = \{right: R, center: C, left: L\}$ identifies the corresponding monitor, and R_{max}
49 is the maximum firing rate to looming stimulus (colored circles in Fig. 6a). Figure 6b shows the value of
50 the response r for each monitor in the 14 neurons studied. It can be observed that the neurons
51 responded intensely to the stimulus presented on each one of the screens surrounding the animal,
52
53
54
55
56
57
58
59
60
61
62
63
64
65

1
2
3
4 suggesting that its receptive field encompasses the entire visual field of the animal and that the firing
5 rate was maximum upon stimulus from the ipsilateral monitor (right).
6
7
8

9 *LSN response to looming stimuli with different dynamics of expansion*

10
11 In a previous section, we showed a preference of the recorded neurons for looming stimuli.
12 Figure 7 shows a typical extracellular recordings, a firing rate response from a typical neuron, and the
13 average firing rate in response to the six looming stimuli described in Table 1, applied to each animal
14 from the right monitor (14 neurons from 9 different animals, one average response per stimulus and per
15 neuron were included in the analyses). For stimuli 1-4 (Table 1), we maintained an approaching speed
16 of $v = 142.5$ cm/s and changed the size of the object l from 8.5 to 64 cm. For stimuli 5-6, we
17 maintained $l = 17$ cm while varying the speed of the object v from 71.5 to 286 cm/s. The firing rate
18 progressively increased as the image of the virtual dark object grew over the retina of the animal.
19 Another feature observed in different recordings to looming stimuli was the existence of a transient
20 component of the response at the beginning of the expansion. This effect could be observed in stimulus
21 4 ($\theta_0 = 14.5^\circ$, see arrow in Fig. 7).
22
23
24
25
26
27
28
29
30

31 Figure 8a shows the average firing rate $R(t)$ as a function of the angular size of the expanding
32 object $\theta(t-\delta_n)$ and in Fig. 8b as a function of the angular velocity of expansion $\theta'(t-\delta_n)$ for the six
33 stimuli from Table 1. The neuronal delay δ_n was assumed to be 40 ms and this assumption was based
34 on the minimum delays of neural phasic responses to changes in luminance (Fig. 3). Comparing Fig.
35 8a-b, we conclude that the spread of the firing rate given an angular size value $\theta(t-\delta_n)$ (vertical dotted
36 line in Fig. 8a) is much larger than the dispersion of the firing rate given the corresponding angular
37 velocity value $\theta'(t-\delta_n)$ (Fig. 8b). Therefore, we next describe the average neural firing rate as a function
38 of the angular velocity using the following phenomenological model, which was adjusted by least
39 squares:
40
41
42
43
44
45
46
47

$$48 \quad R(t) = \frac{R_{\max} \cdot \theta'(t - \delta_n)}{\theta'_{50\%} + \theta'(t - \delta_n)} + R_0$$

49
50
51 The mean absolute error of the fit was 8.1 Hz and the values of the model parameters estimated were:
52 $R_{\max} = 118 \pm 5$ Hz, $\theta'_{50\%} = 192 \pm 4$ °/s and $R_0 = 0.4 \pm 0.1$ Hz (uncertainty of each parameter was
53 obtained using the bootstrap method).
54
55
56
57
58
59
60
61
62
63
64
65

1
2
3
4 It is important to note that the phasic response in the onset of stimulus 4 was only detected at
5 the beginning of the expansion. Figure 8b shows that varying the parameter θ_0 did not have an
6 appreciable influence in the later response to the looming stimulus.
7
8
9

10
11 ***Biologically plausible computational model for spatio-temporal processing and integration in the***
12 ***examined LSNs***
13
14

15 In this section, we propose a biologically plausible computational model that aided us in
16 analyzing the spatio-temporal processing and integration of the examined LSNs. To proposed the
17 model, we used information from studies carried out for more than 40 years in the locust LGMD
18 neuron showing that several biophysical processes operate in parallel to shape and tune the visual
19 response of this LSN (Rowell et al. 1977, Rind and Bramwell 1996, Jones and Gabbiani 2012). To
20 construct the model, we started from a previously proposed model for *Neohelice's* MLG neurons (Oliva
21 and Tomsic 2016), but in this work, we incorporated two improvements: a) the model input was the
22 videos observed by the animal during the electrophysiological experiments; and b) the phenomenon of
23 presynaptic lateral inhibition was incorporated. Figure 9 shows the model for the proposed neural
24 circuitry which is based on the previous models developed for *Neohelice's* MLG1-2 neurons (Oliva and
25 Tomsic 2014, 2016) and the proposed circuit for presynaptic lateral inhibition in the LGMD neuron
26 (Rowell et al. 1977).
27
28
29
30
31
32
33
34
35
36
37

38 *Feed-forward Excitation (FFE) and Inhibition (FFI)*: It is assumed that the circuit presynaptic to the
39 neurons (Fig. 9a) uses as input the sequence of images $I(t)$ having a range of values between 0 and 1.
40 Each photoreceptor senses the image intensity at the position (i,j) (which is discretized to an area of
41 approximately $1.4^\circ \times 1.8^\circ$) and columnar cells produce a signal proportional to the changes of intensity
42 of the image $I_{ij}(t)$ in that region, according to:
43
44
45
46
47
48

$$49 \Delta I_{ij}(t) = I_{ij}(t) - I_{ij}(t - \delta) \quad \text{Eq. 2}$$

50
51 Where δ is the time interval between video frames. Depending on the visual stimuli, the intensity in
52 each column can decrease or increase, and these changes (at position (i,j)) are signaled by two different
53 pathways called $^{off}c_{ij}(t)=\text{poslin}(-\Delta I_{ij}(t))$ and $^{on}c_{ij}(t)=\text{poslin}(\Delta I_{ij}(t))$, where *poslin* represents the positive
54 linear transfer function. In *Neohelice*, this assumption is based on previous observations (Medan et al.
55 2007), in which the intensity and the delay to OFF and ON stimulus were significantly different.
56
57
58
59
60
61
62
63
64
65

As shown in Fig. 6, looming sensitivity for LSNs was intense throughout their large receptive field. Additionally, the sensitivity variation on the stimulation screen (right monitor) was approximately 20%. Consequently, similar to our previous model for MLG2 neurons (Oliva and Tomsic 2016), we assume that the computational model for LSNs in this work does not require the introduction of a receptive field sensitivity function.

Similar to the LGMD model (Rowell et al. 1977, Rind and Bramwell 1996), we assumed that the columnar excitatory channels (producing the FFE) are mutually inhibited through lateral inhibition processes presynaptic to the LSN. Thus, the signal $pre_{ij}(t)$ that descends through the downstream channel (i,j), produces a response that is proportional to the activation of ON/OFF channels (Beron de Astrada et al. 2013) and their response is assumed to be decreased proportionally to a delayed spatial average activity of the neighboring channels in a region of (8×8) channels that were called $a_{ij}(t)$:

$$\begin{aligned}
 pre_{ij}(t) &= poslin({}^{off}c_{ij}(t) + \gamma_1 \cdot {}^{on}c_{ij}(t) - \gamma_2 \cdot a_{ij}(t - \delta_{LI})) \\
 pre_{FFE}(t) &= k_{pre,e} \cdot \sum_{\forall i,j} pre_{ij}(t)
 \end{aligned}
 \tag{Eq. 3}$$

Where pre_{FFE} is the total presynaptic excitation and the coefficient $k_{pre,e}$ is used to normalize the pre_{FFE} signal; $\gamma_{1,2}$ are associated to the weight of ON signals and lateral inhibition, respectively; and δ_{LI} is the delay associated with the lateral inhibition process.

Similar to the LGMD model, it was assumed that the total FFI signal integrates the activity of all the columnar channels according to:

$$pre_{FFI}(t) = k_{pre,i} \cdot \sum_{\forall i,j} ({}^{off}c_{ij}(t) + \gamma_3 \cdot {}^{on}c_{ij}(t))
 \tag{Eq. 4}$$

Where the coefficient $k_{pre,i}$ is used for normalization and γ_3 is a coefficient to be fitted that measures the relative intensity of ON channels with respect to OFF channels.

Similar to previous models for MLG neurons (Oliva and Tomsic 2014; 2016), it is assumed that the release of excitatory neurotransmitters T_{exc} (and inhibitory T_{inh}) from the columnar processes to the LSNs follows first-order dynamics with characteristic time constants τ_{exc} and τ_{inh} according to:

$$\frac{dT_{exc}}{dt} = pre_{FFE}(t - \delta_e) - T_{exc} / \tau_{exc}$$

Eq. 5

$$\frac{dT_{inh}}{dt} = pre_{FFI}(t - \delta_i) - T_{inh} / \tau_{inh}$$

where δ_e and δ_i are the excitatory and inhibitory synaptic latencies, respectively. The excitatory synaptic conductance g_{exc} (and inhibitory g_{inh}) associated with FFE and FFI are given by:

$$g_{exc}(t) = g_{e,max} \frac{T_{exc}(t)}{T_{exc}(t) + T_{exc,50}}$$

Eq. 6

$$g_{inh}(t) = g_{i,max} \cdot T_{inh}(t)$$

where $g_{e,max}$ and $g_{i,max}$ are the maximum total excitatory and inhibitory conductances, respectively. The parameter $T_{exc,50\%}$ corresponds to the value of T_{exc} when g_{exc} reaches 50% of $g_{e,max}$. We approximated the filtered membrane potential $V_{mf}(t)$ to its steady state as:

$$V_{mf}(t) = \frac{(g_{exc}(t)/g_L) \cdot E_{exc} + (g_{inh}(t)/g_L) \cdot E_{inh} + E_L}{(g_{exc}(t)/g_L) + (g_{inh}(t)/g_L) + 1}$$

Eq. 7

where g_L is the leak conductance and E_L , E_{exc} , and E_{inh} are the leak, excitatory, and inhibitory reversal potentials, respectively. Finally, we assumed a covariation between firing rate $R(t)$ and $V_{mf}(t)$ (experimentally observed in Oliva and Tomsic 2014) according to:

$$R(t) = k_R \cdot poslin(V_{mf}(t))$$

Eq. 8

Now that the assumptions of the model have been described, we explain how the simulation is performed: From the videos $I(t)$, the variables $^{off}c_{ij}(t)$ and $^{on}c_{ij}(t)$ were calculated (Eq 2). Then, the total presynaptic signal associated with the FFE and the FFI ($pre_{FFE}(t)$ and $pre_{FFI}(t)$) were obtained using Eqs. 3 and 4. The integration of Eq. 5 was performed using the forward Euler method and the excitatory and inhibitory conductances (g_{exc} and g_{inh}) were calculated according to Eq. 6. Finally, the filtered membrane potential, V_{mf} , and the firing rate, R , were obtained using Eqs. 7-8, respectively.

Parameter selection and model fit

The model presented in the previous section determined a nonlinear spatio-temporal filter acting on the sequence of images $I(t)$ seen by the animal during the electrophysiological experiments and had a wide set of parameters that must be fitted to reproduce the firing rate measured experimentally.

1
2
3
4 Similar to previous work (Oliva and Tomsic 2014), we assumed the resting membrane potential $E_L=0$
5 mV, the excitatory synaptic reversal potential $E_{exc}=60$ mV, and inhibitory synaptic reversal potential
6 $E_{inh}=-3$ mV. The signals $pre_{FFE}(t)$ and $pre_{FFI}(t)$ were normalized to the maximum value reached for all
7 stimuli. To meet this condition, the constants $k_{pre,e}=0.0033$ and $k_{pre,i}=0.0011$ were used. All the
8 remaining parameters of the model were estimated by nonlinear square error minimization between the
9 experimental average firing rate and the model prediction. For this, we used a nonlinear least squares
10 method to fit the experimental measurements (*patternsearch* algorithm in Matlab). The values obtained
11 for the estimated parameters were: firing rate constant $k_R=4$ Hz, excitatory and inhibitory time
12 constants and delays $\tau_{exc}=40$ ms, $\tau_{inh}=777$ ms, $\delta_e=40$ ms, $\delta_i=80$ ms, and $\delta_{LI}=40$ ms. The parameters
13 related to synaptic conductances were: $(g_{exc,max}/g_L)=8.3$, $(g_{inh,max}/g_L)=7.5$, $T_{exc,50\%}=0.48$, $T_{inh,50\%}=$
14 0.04 . Because the ‘maximum normalized excitatory and inhibitory conductance’ were referred to the
15 leak conductance, they are dimensionless. Finally, the adimensional parameters that measure the
16 relative influence of the ON units were: $\gamma_1=0.5$, $\gamma_3=2.78$; and for the lateral inhibition influence $\gamma_2=$
17 1.69 .

18
19
20
21
22
23
24
25
26
27
28
29
30 As shown in Fig. 10 (red traces), through optimizing these parameters, a satisfactory fitting can
31 be achieved throughout all stimuli (the mean absolute error of the fit was 2.3 Hz), showing that the
32 biologically inspired model is useful for capturing the relevant aspects of the LSN response.

33
34
35
36
37
38
39
40
41
42
43
44
45
46
47
48
49
50
51
52
53
54
55
56
57
58
59
60
61
62
63
64
65
Next, we analyzed how the model responds to the same visual stimuli without the presence of
presynaptic lateral inhibition (LI). For this, we compared the predictions of the model described above
(with LI, red lines in Fig. 10) with the predictions of another model in which we set the parameter $\gamma_2=$
0 (canceling the inhibitory influence produced by the activity of the neighboring channels $a_{ij}(t)$ in Eq.
3). Therefore, this second model is equivalent to the one proposed in Oliva and Tomsic 2016) where
only FFE and FFI acted. Canceling only the parameter γ_2 results in a generalized increase in the
response. Therefore, to optimize the predictions of the model without lateral inhibition, the parameter
 $(g_{inh,max}/g_L)$ was again adjusted to the value: $(g_{inh,max}/g_L)=11$. The results of adjusting the model
without lateral inhibition are shown in Fig. 10 (green traces). The mean absolute error of the fit was 4.1
Hz. In Fig. 10a, it is observed that the model without LI overestimates the neuronal activity to an
OPTO stimulus. In Fig. 10b, it is observed that for the LOOM-P stimulus, readjusting the maximum
conductance associated with the FFI compensates for the absence of the LI. For the case of the
RECED-P stimulus, increasing the FFI does not compensate for the absence of the LI, and the model
without LI overestimates the activity. Finally, for the looming stimuli (Fig. 10c) it is observed that the

1
2
3
4 model without LI overestimates the response, mainly at the beginning of the expansion (when the
5 angular velocities are low).
6
7
8
9

10 11 12 13 **DISCUSSION** 14

15 16 17 *Spatio-temporal processing and integration in LSNs*

18
19 Due to the biological relevance of collision avoidance behaviors, there is a great interest in
20 understanding how visual sensory circuits encode looming stimuli and what is the spatio-temporal
21 processing and integration that tune LSNs to these stimuli. To date, the most complete answers to these
22 questions have been obtained in the LGMD neuron of the locust. The main conclusion has been that
23 several biophysical processes operate in parallel to shape the visual response of the LSNs (reviewed in
24 Oliva 2015). These processes include: A) the dynamic balance between feed-forward excitation and
25 feed forward inhibition; in which both processes are fed by the activity of columnar information
26 channels with non-directional information (Rind and Bramwell 1996, Jones and Gabbiani 2010); B) the
27 lateral inhibition between neighboring columnar channels that would protect LSNs from habituation by
28 the dense optical flow produced in the animal's eye by movement of the animal itself (O'Shea and
29 Rowell 1975, Rind and Bramwell 1996, Gabbiani et al. 2002), and C) adaptation processes inhibiting
30 their response to stimuli that are constant over time (Peron and Gabbiani 2009).
31
32
33
34
35
36
37
38
39
40

41 In the first part of this work, we used extracellular recordings to exhaustively characterize
42 MSNs' response against a wide range of optical flow patterns, showing that they were highly sensitive
43 to looming stimuli, and therefore could be classified as LSNs. The neuronal responses for the LSNs
44 recorded in this work showed important similarities to those previously measured for the MLG2
45 neurons in *Neohelice* (Oliva and Tomsic 2016). These similarities were: a) a rather uniform looming
46 sensitivity throughout a large receptive field, b) a higher response to looming, rather than to receding
47 stimuli (Fig. 5b in this work) and (Oliva et al. 2007), c) the firing rate of the LSNs can be described as
48 function of the angular velocity θ' (Fig. 8b), d) phasic responses to changes in luminance (Fig. 3) and
49 also at the beginning of looming stimuli with θ_0 greater than 14° (Oliva and Tomsic 2016), and e) a
50 reduction of response to OPTO stimulus, (Fig. 4c in this work) and (Medan et al. 2007).
51
52
53
54
55
56
57
58
59
60
61
62
63
64
65

1
2
3
4 In the second part of this work, we proposed a computational model consistent with the
5 previous results and models for *Neohelice's* lobula giant neurons and for the locust's LGMD neuron.
6 The model presented in this work represented a simplification in relation to the models with greater
7 physiological realism for the LGMD (Rind and Bramwell 1996, Jones and Gabbiani 2012).
8 Nevertheless, this simplification allowed us to optimize the parameters by least squares to adjust the
9 predictions of the model to the experimental measurements, and as we show in the next section, to
10 analyze the physiological processing acting in parallel in the examined LSNs.
11
12
13
14
15
16
17
18

19 ***Neuronal response to changes in luminance***

20 The first experiment studied the neuronal response to local changes in luminance (Fig. 3). A
21 phasic response was observed, which is a characteristic property of *Neohelice's* MLGs neurons in crabs
22 (Beron Astrada and Tomsic 2002, Oliva and Tomsic 2014, 2016) and in the locust LGMD neuron
23 (Rowell et al. 1977). As shown in Fig. 3b, the neuronal response even showed a sensitivity to stimuli
24 that activate no more than a dozen ommatidia. According to the model proposed in Fig. 9, the phasic
25 response was a consequence of the action of fast feed-forward excitation (whose intensity was
26 proportional to the number of activated columnar channels) and the delayed slow feed-forward
27 inhibition that canceled subsequent neuronal activity. This response can be interpreted as a local
28 estimation of the system's temporal impulse response, and according to the model, the dynamic balance
29 between FFE and FFI produces a high-pass filtering mechanism. This effect (added to the rectification
30 for the firing rate in Eq. 8) generates one of the mechanisms for the selectivity to the looming stimuli.
31
32
33
34
35
36
37
38
39
40
41

42 ***Moving stimuli that highlighted different components of the OF***

43 The study of neuronal responses to moving stimuli comprised the analysis of two different
44 components of the optical flow. First, optical flows associated with rotating edges movements (denoted
45 as ROF). These flows would be generated if the animal revolved around its vertical axis and observed
46 fixed edges, or conversely, if the animal was fixed with rotating edge movement around its vertical axis
47 with constant angular velocity. Second, the translational optical flow of expansion or contraction
48 (denoted as TOF) that would be generated if an object was approaching (or moving away from) the
49 fixed animal. This flow may also occur if the animal approaches (or moves away from) from fixed
50 objects in the environment. In addition, for ROF and TOF, two basic conditions were simulated: sparse
51 optical flows (stimuli ME(1-3), LOOM, and RECED) that would be generated if the animal interacted
52
53
54
55
56
57
58
59
60
61
62
63
64
65

1
2
3
4 with a single object, and also the dense optical flow that would appear if the animal interacted with
5 many objects (OPTO, LOOM-P and RECED-P), see Fig. 1.
6
7
8

9
10 ***Neuronal response to ROF***

11 Stimuli characteristic of an ROF were ME (1-3) and OPTO (Fig. 1a). Fig. 4a shows that the
12 firing rate started with a peak and then decreased. Comparisons of responses throughout stimulation
13 showed that the stimulus OPTO produced a significantly lower response, in which after the initial peak,
14 the firing rate decreased toward the baseline near zero (Fig. 4c). In the case of ME (1-3), the firing rate
15 remained constant at higher steady values (lower than the peak). According to the model proposed in
16 Fig. 9, the drop in the firing rate was due to the action of two effects: the dynamic balance between
17 feedforward excitation and a delayed inhibition (Fig. 9c); and also as a consequence of lateral
18 inhibition between the excitatory columnar channels.
19
20
21
22
23
24
25

26 In relation to the response to OPTO stimulus, our model attributed the reduction of its initial
27 peak response to the delayed lateral inhibition mechanism (O'Shea and Rowell 1975; Rind and
28 Bramwell 1996; Gabbiani et al. 2002; Rind et al. 2016). Under this assumption, the moving dark and
29 white bars of this stimulus would produce an inhibitory effect among the neighboring activated
30 columnar channels presynaptic to LSNs, thereby decreasing the firing rate (Fig. 9b, panel (iv)).
31 Therefore, in contrast to neurons involved in optomotor response behaviors, such as those broadly
32 studied LPNs in the fly (Borst and Haag 2002), the recorded neurons had a weak response to wide-field
33 motion (Rind and Simmons 1992, Medan et al. 2007).
34
35
36
37
38
39
40

41 In relation to the directionality of neural responses, the studied LSNs showed no significant
42 differences between ME (1-3) stimuli. This indicates that the measured neurons did not have a
43 preferred direction in their response, which is in agreement with the type of response also measured in
44 insect LSNs (Krapp and Gabbiani 2005, Yamawaki and Toh 2009, Jones and Gabbiani 2010).
45 According to the model (Eq. 2), this is a consequence of the FFE being fed by the activity of columnar
46 information channels signaling the change in luminance without directional information (Rind and
47 Bramwell 1996, Jones and Gabbiani 2010).
48
49
50
51
52
53

54 ***Neuronal response to TOF***

55
56 The other group of visual stimuli analyzed in this work consisted of sparse (or dense) optical
57 flows of expansion and contraction, corresponding to the stimuli LOOM, RECED, LOOM-P, and
58 RECED-P (Fig. 1b-c). By comparing the maximum firing rates for these four stimuli, we found that the
59
60
61
62
63
64
65

1
2
3
4 looming response was significantly greater (Fig. 5b). In particular, the LOOM response was
5 significantly higher than that of RECED. This result indicates that the measured MSNs reflected the
6 most relevant property of LSNs, which is their preferential response to looming stimuli, rather than to
7 receding stimuli (Oliva et al. 2007).
8
9

10
11 Previous phenomenological studies to characterize LSNs have been carried out in different
12 animal species using input-output functions of the type $R(t)=g(z(t-\delta_n))$. Where z is an input optical
13 variable, $R(t)$ is the neuronal firing rate, δ_n is the delay time and g a nonlinear function. The most
14 commonly used optical variables are the angular velocity $\theta'(t)$ and the angular size $\theta(t)$. Using this
15 information, an animal could compute in parallel several other variables of interest, such as the time to
16 collision $\tau=\theta/\theta'(t)$ and $\eta= \theta' \cdot e^{-\alpha\theta}$, which is called the η function (Laurent and Gabbiani 1998). These
17 results show that animal's brain can reconstruct approaching objects using several computations in
18 which each variable provides a different piece of information about the state of the environment, and
19 the animal presumably makes an informed decision based on these different inputs. As shown in Fig. 8,
20 the firing rate of the LSNs measured in this work can be described phenomenologically as a function of
21 the angular velocity θ' and therefore can be classified as ρ -type neurons (Laurent and Gabbiani 1998).
22 In this way, the computation performed by these neurons only contemplates a part of the computation
23 of the variable $\eta= \theta' \cdot e^{-\alpha\theta}$ that the LGMD neuron performs.
24
25

26 Although the phenomenological model satisfactorily describes the response of LSNs to looming stimuli
27 and is useful for correlating neuronal activity with behavior (Oliva and Tomsic 2016), there is interest
28 in studying which physiological processes shape the responses of the LSNs, using detailed
29 computational models such as those developed for the LGMD neuron (Rind and Bramwell 1996, Jones
30 and Gabbiani 2012) to predict the neuronal response against more complex spatio-temporal patterns of
31 activation in the ommatidia arrangement. A first effect not considered by the phenomenological model
32 is related to the phasic responses observed at the beginning of the expansion in the looming stimulus 4
33 (indicated by an arrow in Fig. 7). According to the proposed model, the phasic response for looming
34 stimuli is a consequence of fast feed-forward excitation and the delayed slow feed-forward inhibition
35 that reduces subsequent neuronal activity. As size and angular velocity increase during the expansion,
36 the excitation increases and the firing rate again grows until the expansion ends. According to the
37 model, the transient effect at the beginning of the expansion has a similar cause to that observed for the
38 beginning of the stimulus ME-1 in Fig. 9c and can be explained due to the same balance between
39 excitatory and inhibitory conductance dynamics.
40
41
42
43
44
45
46
47
48
49
50
51
52
53
54
55
56
57
58
59
60
61
62
63
64
65

1
2
3
4 When comparing the neuronal maximum firing rate for the two stimuli of expansion (LOOM
5 and LOOM-P), we found that there were significant differences in favor of LOOM. This result
6 contrasts with results of studies in other crabs (Horseman et al. 2011), in which the visual sensitivity of
7 a set of MSNs was locally measured and a typical response of a matched filter was found, that would
8 imply a maximum response to the LOOM-P stimuli. According to the model presented in this work, the
9 declining response to LOOM-P stimulus (relative to LOOM) observed in the measured LSNs was a
10 consequence of feed-forward and lateral inhibition that would reduce the response to dense optical flow
11 of expansion. Similar to what was found for the OPTO stimulus, lateral inhibition would protect the
12 habituation of LSNs to the optical flow of expansion and contraction generated by the movement of the
13 animal in a rich-textured environment.
14
15

16
17
18
19
20
21
22 Another important effect observed in responses to LOOM-P and RECED-P stimuli was an
23 abrupt oscillation of the firing rate at a frequency of 1 Hz (Fig. 5a). These peaks of activity were
24 synchronized with the expansion/contraction of the larger dark square border (Fig. 1c). The response
25 peaks upon exposure to the LOOM-P stimulus were greater than those in response to RECED-P,
26 because the LOOM-P stimulus comprised a sequence of looming stimuli, while the RECED-P was
27 composed of a sequence of receding stimuli. However, it should be noted that although the model
28 predicted the existence of peaks in the firing rate, the fitting of the activity slightly overestimated the
29 response to the LOOM-P and RECED-P stimuli (Fig. 10b). We attribute this problem to the fact that
30 the proposed model did not incorporate the aforementioned phenomenon of adaptation (Peron and
31 Gabbiani 2009) and also the phenomenon of short-term habituation observed in presynaptic columnar
32 channels to MSNs (Beron de Astrada et al. 2013).
33
34
35
36
37
38
39
40
41
42

43 Beyond the above, we consider that the model proposed in this work allows the capture of
44 relevant aspects of the visual response in the context of collision avoidance for a group of LSNs in
45 *Neohelice*, and also suggests that the computation performed by these neurons in a decapod crustacean
46 appears to be based on similar physiological processing previously described for the LGMD in insects.
47
48
49
50

51 ***Usefulness of extracellular techniques for neuroethological studies***

52
53 The use of the extracellular technique allowed us to obtain prolonged stable records of about 5
54 hours, aiding the characterization of the neuronal response to a broad set of visual stimuli to analyze the
55 spatio-temporal processing and integration in LSNs. However, to identify each specific neuronal type
56 in relation to previous identifications based on intracellular recordings and stains (Tomsic et al., 2017),
57
58
59
60
61
62
63
64
65

1
2
3
4 further studies involving simultaneous intracellular and extracellular measurements of LSN responses
5 are needed. Another technique that could be used for the identification of the recorded neurons is the
6 one proposed by Kostarakos and Hedwig (2017), whose responses are recorded extracellularly and can
7 be identified using the same suction electrodes to deliver fluorescent tracers into the nervous system by
8 means of electrophoresis, allowing retrograde labeling. Finally, the last reason justifying the usefulness
9 of extracellular techniques on the surface of the optic nerve is the interest of understanding how the
10 LSNs regulate the visually guided collision avoidance behaviors. Two previous studies in freely-
11 behaving insects that analyzed this point were performed in locusts using an experimental preparation
12 that allowed the study of the relationship between the DCMD's activity by surface extracellular
13 recordings with hook electrodes in the optic tract, the electromyographic activity measurements in
14 muscles, and the behavioral response (Santer et al. 2008, Fotowat et al. 2011). As shown in this work,
15 the possibility of making surface extracellular recordings of LSNs from *Neohelice's* optic nerve is an
16 indication of the feasibility of further studies similar to those conducted in locusts.
17
18
19
20
21
22
23
24
25
26
27
28
29
30

31 **CONFLICT OF INTEREST**

32
33
34 The authors declare no competing or financial interests.
35
36

37 **ETHICAL STANDARD**

38
39 All experiments on animals described above were performed in accordance with applicable
40 national legislation and institutional guidelines for the care and use of animals.
41
42
43

44 **ACKNOWLEDGEMENTS**

45
46 We thank D. Tomsic, M. Berón de Astrada and F. Magani for fruitful discussions and
47 corrections to this manuscript. This work describes research partially funded by National Council of
48 Scientific and Technical Research (CONICET), National Agency of Science and Technology
49 (ANPCyT), grant number PICT 2012-2765.
50
51
52
53
54
55
56
57
58

59 **REFERENCES**

60
61
62
63
64
65

- 1
2
3
4
5
6 -Berón de Astrada M, Tomsic D (2002) Physiology and morphology of visual movement detector
7 neurons in a crab (Decapoda: Brachyura). *J Comp Physiol A* 188:539-551. doi: 10.1007/s00359-002-
8 0328-4
9
10
11 -Berón de Astrada M, Bengochea M, Medan V, Tomsic D (2012) Regionalization in the eye of the
12 grapsid crab *Neohelice granulata* (=Chasmagnathus granulatus): variation of resolution and facet
13 diameters. *J Comp Physiol A* 198:173–180. doi: 10.1007/s00359-011-0697-7
14
15 -Berón de Astrada M, Bengochea M, Sztarker J, Delorenzi A, Tomsic D (2013) Behaviorally related
16 neural plasticity in the arthropod optic lobes. *Current Biology* 23:1389-1398. doi:
17 10.1016/j.cub.2013.05.061
18
19
20
21 -Borst A, (1991) Fly visual interneurons responsive to image expansion. *Zool Jb Physiol* 95:305-313
22
23 -Borst A, Haag J (2002) Neural networks in the cockpit of the fly. *J Comp Physiol A* 188: 419–437.
24 doi: 10.1007/s00359-002-0316-8
25
26 -Dunn TW, Gebhardt C, Naumann EA, Riegler C, Ahrens MB, Engert F, Del Bene F (2016) Neural
27 circuits underlying visually evoked escapes in larval zebrafish. *Neuron* 89:613-628.
28 doi: <http://dx.doi.org/10.1016/j.neuron.2015.12.021>
29
30
31
32 -Fotowat H, Gabbiani F (2011) Collision Detection as a Model for Sensory-Motor Integration. *Annu*
33 *Rev Neurosc* 4:1–19. doi:10.1146/annurev-neuro-061010-113632
34
35 -Fotowat H, Harrison R, Gabbiani F (2011) Multiplexing of Motor Information in the Discharge of a
36 Collision Detecting Neuron during Escape Behaviors. *Neuron* 69:147–158. doi:
37 10.1016/j.neuron.2010.12.007
38
39
40
41 -Gabbiani F, Krapp HG, Laurent G (1999) Computation of object approach by a wide field, motion-
42 sensitive neuron. *J Neuroscience* 19:1122–1141
43
44 -Gabbiani F, Krapp HG, Koch C, Laurent G (2002) Multiplicative computation in a visual neuron
45 sensitive to looming. *Nature* 21:320–324. doi: 10.1038/nature01190
46
47
48 -Glantz RM (1974) Defense reflex and motion detector responsiveness to approaching targets: the
49 motion detector trigger to the defense reflex pathway. *J Comp Physiol* 95:297-314
50
51
52 -Gray JR, Blincow E, Robertson RM (2010) A pair of motion-sensitive neurons in the locust encode
53 approaches of a looming object. *J Comp Physiol A* 196:927-938. doi: 10.1007/s00359-010-0576-7
54
55
56 -Hemmi JM, Tomsic D (2012) The neuroethology of escape in crabs: from sensory ecology to neurons
57 and back. *Curr Opin Neurobiol* 22:194–200. doi: 10.1016/j.conb.2011.11.012
58
59
60
61
62
63
64
65

- 1
2
3
4 -Horseman BG, Macauley MW, Barnes WJP (2011) Neuronal processing of translational optic flow in
5 the visual system of the shore crab *Carcinus maenas*. *Journal of Experimental Biology* 214(9): 1586-
6 1598.
7
8
9
10 -Jones PW, Gabbiani F (2010) Synchronized neural input shapes stimulus selectivity in a collision-
11 detecting neuron. *Current Biology* 20(22): 2052-2057.
12
13 -Jones PW, Gabbiani F (2012) Logarithmic compression of sensory signals within the dendritic tree of
14 a collision-sensitive neuron. *Journal of Neuroscience* 32(14): 4923-4934.
15
16
17 -Kostarakos K, Hedwig B (2017) Surface electrodes record and label brain neurons in insects. *J*
18 *Neurophysiol.* doi: 10.1152/jn.00490.2017
19
20 -Krapp HG, Hengstenberg R (1996) Estimation of self-motion by optic flow processing in single visual
21 interneurons. *Nature* 384:463-466. doi: 10.1038/384463a0
22
23
24 -Krapp HG, Gabbiani F (2005) Spatial distribution of inputs and local receptive field properties of a
25 wide-field, looming sensitive neuron. *J Neurophysiol* 93:2240–53. doi: 10.1152/jn.00965.2004
26
27 -Laurent G, Gabbiani F (1998) Collision-avoidance: nature’s many solutions. *Nat. Neurosci.* 1:261–63
28
29 -Medan V, Oliva D, Tomsic D (2007) Characterization of Lobula Giant neurons responsive to visual
30 stimuli that elicit escape reactions in the crab *Chasmagnathus*. *J of Neurophys* 98:2414-2428. doi:
31 10.1152/jn.00803.2007
32
33
34
35 -Nelson RC, Aloimonos J (1988) Finding motion parameters from spherical motion fields (or the
36 advantages of having eyes in the back of your head). *Biological cybernetics* 58:261-273.
37
38 -Nilsson DE, Osorio D (1998) Homology and parallelism in arthropod sensory processing. In
39 *Arthropod relationships*. Springer Netherlands. pp. 333-347
40
41
42 -Oliva D, Medan V, Tomsic D (2007) Escape behaviour and neuronal responses to looming stimuli in
43 the crab *Chasmagnathus granulatus* (Decapoda: Grapsidae). *J Exp Biol* 210:865-880. doi:
44 10.1242/jeb.02707
45
46
47 -Oliva D, Tomsic D (2014) Computation of object approach by a system of visual motion-sensitive
48 neurons in the crab *Neohelice*. *J Neurophysiol* 112:1477-1490. doi:10.1152/jn.00921.2013
49
50
51 -Oliva D (2015) Collision Avoidance Models, Visually Guided. In: *Encyclopedia of Computational*
52 *Neuroscience* (ed. Jaeger D. and Jung R.), Springer-Verlag Berlin Heidelberg, pp 626-645
53
54 -Oliva D, Tomsic D (2016) Object approach computation by a giant neuron and its relationship with
55 the speed of escape in the crab *Neohelice*. *Journal of Experimental Biology.* 219:3339-3352.
56
57
58
59 doi: 10.1242/jeb.136820
60
61
62
63
64
65

- 1
2
3
4 -O'Shea M, Rowell CHF (1975) Protection from habituation by lateral inhibition. *Nature* 254:53–55.
5
6 -Peron SP, Gabbiani F (2009) Spike frequency adaptation mediates looming stimulus selectivity in a
7 collision detecting neuron. *Nat. Neurosci* 12:318–326. doi:10.1038/nn.2259
8
9 -Preuss T, Osei-Bonsu PE, Weiss SA, Wang C, Faber DS (2006) Neural representation of object
10 approach in a decision-making motor circuit. *Journal of Neuroscience* 26:3454-3464.
11
12 doi:10.1523/JNEUROSCI.5259-05.2006
13
14 -Quiari Quiroga R (2007) *Scholarpedia*, 2(12):3583. doi:10.4249/scholarpedia.3583
15
16 -Quiroga RQ, Nadasdy Z, Ben-Shaul Y (2004) Unsupervised spike detection and sorting with wavelets
17 and superparamagnetic clustering. *Neural computation* 16:1661–1687.
18
19 doi:10.1162/089976604774201631
20
21 -Rind FC, Bramwell DI (1996) Neural network based on the input organization of an identified neuron
22 signaling impending collision. *J Neurophysiol* 75:967–985
23
24 -Rind FC, Simmons PJ (1992) Orthopteran DCMD neuron: a reevaluation of responses to moving
25 objects. I. Selective responses to approaching objects. *J Neurophysiol* 68:1654–66
26
27 -Rind FC, Simmons PJ (1999) Seeing what is coming: building collision-sensitive neurones. *Trends*
28 *Neurosci* 22:215-20
29
30 -Rind FC, Wernitznig S, Pölt P, Zankel A, Gütl D, Sztarker J, Leitinger G (2016). Two identified
31 looming detectors in the locust: ubiquitous lateral connections among their inputs contribute to
32 selective responses to looming objects. *Scientific Reports*, 6:35525. doi: 10.1038/srep35525
33
34 -Rosner R, Homberg U (2013) Widespread sensitivity to looming stimuli and small moving objects in
35 the central complex of an insect brain. *Journal of Neuroscience* 33(19): 8122-8133
36
37 -Rowell CF, O'Shea M, Williams JL (1977) The neuronal basis of a sensory analyser, the acridid
38 movement detector system. IV. The preference for small field stimuli. *Journal of Experimental Biology*
39 68:157-185
40
41 -Santer RD, Yamawaki Y, Rind FC, Simmons PJ (2008) Preparing for escape: an examination of the
42 role of the DCMD neuron in locust escape jumps. *J Comp Physiol A* 194:69–77. doi: 10.1007/s00359-
43 007-0289-8
44
45 -Srinivasan MV, Zhang S (2004) Visual motor computations in insects. *Annu Rev Neurosci* 27:679-
46 696. doi: 10.1146/annurev.neuro.27.070203.144343
47
48 -Strausfeld NJ (2005) The evolution of crustacean and insect optic lobes and the origins of chiasmata.
49 *Arthropod Struct Dev* 34:235-256
50
51
52
53
54
55
56
57
58
59
60
61
62
63
64
65

1
2
3
4 -Sztarker J, Strausfeld NJ, Tomsic D (2005) Organization of optic lobes that support motion detection
5 in a semiterrestrial crab. *J Comp Neurol* 493:396-411. doi: 10.1002/cne.20755
6
7 -Tomsic D, Sztarker J, Beron de Astrada MB, Oliva D, Lanza E (2017) The predator and prey
8 behaviors of crabs: from ecology to neural adaptations. *Journal of Experimental Biology* 220(13):
9 2318-2327.
10
11 -Wang Y, Frost BJ (1992) Time to collision is signalled by neurons in the nucleus rotundus of pigeons.
12 *Nature* 356:236-238. doi: 10.1038/356236a0
13
14 -Wasserman L (2004) All of Statistics. A concise course in Statistical inference. Springer.
15
16 -Wild J, Prekopcsak Z, Sieger T, Novak D, Jech R (2012) Performance comparison of extracellular
17 spike sorting algorithms for single-channel recordings. *Journal of Neuroscience Methods* 203:369-376.
18 doi: 10.1016/j.jneumeth.2011.10.013
19
20 -Yamawaki Y, Toh Y (2009) Responses of descending neurons to looming stimuli in the praying
21 mantis *Tenodera aridifolia*. *J Comp Physiol A* 195:253–264. doi: 10.1007/s00359-008-0403-6
22
23
24
25
26
27
28
29
30
31

FIGURE LEGENDS:

32
33
34 **Fig. 1** Visual Stimuli. **(a)** Moving Edges (ME1-3): (i-iii) A dark edge moved at constant angular
35 velocity in three different directions $\omega = \theta' = 26$ °/s. (iv) OPTO: An optomotor pattern moved at
36 constant angular velocity ($\Delta\phi = 12^\circ$, $\omega = 26$ °/s) **(b)** Looming and receding corresponded to sparse
37 translational optical flow (TOF) of expansion and contraction. (i) LOOM or looming stimuli: l was the
38 half-size of the object, v was the approach speed, L was the initial distance and θ is the angular size of
39 the object in degrees. (ii) RECED or receding stimulus. **(c)** (i) Simulation of the animal moving
40 through a tunnel of 4 cm width at a speed of 17 cm/s. The spatial period of the white and black bands
41 was $\lambda = 17$ cm. Looming and receding patterns correspond to dense TOF of expansion and contraction.
42 The simulation was generated by a superposition of loomings or recedings. (ii) LOOM-P: visual stimuli
43 observed in the direction of movement. (iii) RECED-P: visual stimuli observed in the opposite
44 direction to the movement
45
46
47
48
49
50
51
52
53
54

55 **Fig. 2** Electrophysiology. **(a)** The animal was located in the center of the setup and immobilized by its
56 carapace. The statocyte was removed and a suction electrode made contact with the optic nerve. PC2
57 recorded the electrophysiological activity and PC1 emitted a synchronization signal to PC2 via an
58
59
60
61
62
63
64
65

1
2
3
4 auxiliary wire, which allowed the synchronization of recordings in PC2 with the visual stimulation
5 produced by PC1. (b) Typical extracellular recordings (gray traces) in response to looming stimulus
6 number 2 (Table 1) alternately applied on the three screens around the animal. Three spikes' classes
7 were detected (for details of the spike sorting method, see the Data analysis section). The black curved
8 line at the bottom of the panel represents the angular size, $\theta(t)$, of the looming stimulus. Vertical dashed
9 lines signal the beginning of the stimulus. (c) Isolated spikes detected by spike sorting process. In this
10 recording, the spike sorting algorithm found three neuronal classes
11
12
13
14
15
16
17
18

19 **Fig. 3** Neuronal response to changes in luminance. Dark square figures of different angular sizes θ
20 were applied. (a) Upper traces: extracellular recording from a single animal illustrating the types of
21 responses. In these recordings, the spike sorting algorithm found two neuronal classes. The gray
22 horizontal line at the bottom of each panel represents the stimulation. Vertical dashed lines signal the
23 beginning of the stimulus. (b) Average number of spikes emitted in a time window of 0.5 s after the
24 luminance change (14 neurons from 9 different animals (one average response per stimulus and per
25 neuron were included). The error bars represent mean \pm SD. The black curve corresponds to the fit by
26 least squares according to $R(\theta) = \alpha \cdot (\theta - \beta)^{\gamma}$
27
28
29
30
31
32
33

34 **Fig. 4** Neuronal response to dark moving edges and optomotor stimuli. (a) Upper traces: A typical
35 extracellular recording from a single animal illustrating the type of responses. In these recordings, the
36 spike sorting algorithm found three neuronal classes. Second traces: peristimulus time histograms
37 (black thin trace) showing a typical response from a single neuron. Third traces: peristimulus time
38 histograms showing the average spike rate (black trace) from 14 neurons from 9 different animals (one
39 average response per stimulus and per neuron were included in the analyses). The gray bands represent
40 the standard deviation around the mean. The horizontal gray line at the bottom of each panel represents
41 the stimulation. (b) Mean maximum firing rate during stimulation. Error bars represent mean \pm SD. No
42 significant differences were observed. (c) The mean firing rate during stimulation showed that the
43 response to the stimulus OPTO was significantly lower
44
45
46
47
48
49
50
51
52
53

54 **Fig. 5** Neuronal response to sparse (and dense) optical flow of expansion and contraction. (a) Upper
55 traces: A typical extracellular recording from a single animal illustrating the type of responses. Second
56 traces: peristimulus time histograms (black thin trace) showing a typical response from a single neuron.
57 Third traces: peristimulus time histograms showing the average spike rate (black thin trace) from 14
58
59
60
61
62
63
64
65

1
2
3
4 neurons from 9 different animals. The gray bands represent the standard deviation around the mean.
5
6 The black curved lines at the bottom of each panel represent the stimulation. **(b)** The maximum firing
7
8 rate produced by each stimulus. Error bars represent mean \pm SD
9

10
11 **Fig. 6** Neuronal responses to looming stimuli from different approaching directions. **(a)** A typical LSN
12
13 peristimulus histogram in response to looming stimulus number 2 presented on the different monitors.
14
15 The small colored circles represent the maximum firing rate, R_{max} , to looming stimulus in each screen.
16
17 Each color represents one direction of approach in Fig. 2a (right: blue, center: black, left: red). **(b)** LSN
18
19 response magnitude r for the 14 recorded neurons. The standardized response r was defined as $r(n) =$
20
21 $R_{max}(n)/R_{max}(R)$, where $n = \{R, C, L\}$ identifies the corresponding monitor (see Fig. 2a)
22
23

24
25 **Fig. 7** Neuronal response to looming stimuli with different dynamics of expansion (see Table 1). Upper
26
27 traces: A typical extracellular recording from a single animal illustrating the type of responses. Second
28
29 traces: peristimulus time histograms (black thin trace) showing a typical response from a single neuron.
30
31 Third traces: peristimulus time histograms showing the average spike rate. The gray bands represent
32
33 the standard deviation around the mean. The gray curved lines at the bottom of each panel represent the
34
35 angular size, $\theta(t)$, of the looming stimulus. Vertical dashed lines signal the beginning of the stimulus
36
37 expansion. The arrow shown in the response to stimulus 4, indicates the phasic response observed at
38
39 the beginning of the expansion
40

41
42 **Fig. 8** Average firing rate and phenomenological model for the LSNs responses to looming stimuli.
43
44 Data obtained for the six stimuli of Table 1 (gray traces) plotted as a function of two different optical
45
46 variables: **(a)** angular size θ , **(b)** angular velocity θ' . Black lines correspond to the fits using the
47
48 phenomenological model
49

50
51 **Fig. 9** Biologically inspired computational model of LSNs. **(a)** Schematic diagram of the neural
52
53 circuitry thought to be operating in the examined LSN neurons inspired by the qualitative LGMD
54
55 model (Rowell et al. 1977), and the quantitative models proposed by Rind and Bramwell (1996) and
56
57 Jones and Gabbiani (2012). Open circles and triangles represent excitatory and inhibitory synapses,
58
59 respectively. Each columnar channel produced a signal proportional to the ON and OFF changes of
60
61 intensity of the image through the $^{on}c_{ij}(t)$ and $^{off}c_{ij}(t)$ units, respectively. These signals go down through
62
63
64
65

1
2
3
4 the excitatory columnar processes (vertical black lines) that are mutually inhibited by lateral inhibition
5 (LI, horizontal gray lines). This information is spatially integrated to produce the excitatory synaptic
6 conductance $g_{exc}(t)$ associated with FFE (see Eqs. 3,5-6). On the other hand, the FFI is generated from
7 the spatial integration of the columnar information producing the inhibitory synaptic conductance
8 $g_{inh}(t)$ (see Eqs. 4,5-6). The dynamic balance of synaptic excitation and inhibition determines the
9 membrane potential $V_{mf}(t)$ (Eq. 7), which co-vary with the firing rate $R(t)$ (Eq. 8). **(b)** Each image
10 represents the activation of the columnar channels of the circuit. (i) Moving image $I_{ij}(t)$ which is the
11 input of the model. (ii) Activation of the $^{on}c_{ij}$ columnar channels that sense the OFF-> ON transitions in
12 luminance. (iii) Activation of the $^{off}c_{ij}$ columnar channels that sense the ON-> OFF transitions. (b.iv)
13 Activation of the pre_{ij} channels without applying the $poslin$ function to assess the influence of lateral
14 inhibition (Eq. 3). **(c)** Temporal evolution of the model variables. (i) Moving image $I_{ij}(t)$ at the input of
15 the model. (ii) Temporal evolution of the excitatory and inhibitory normalized conductances (Eq. 6).
16 (iii) Temporal evolution of the firing rate (Eq. 8)

17
18
19
20
21
22
23
24
25
26
27
28
29
30 **Fig. 10** Average data and model fits of the firing rate of LSNs. Peristimulus time histograms (black
31 traces) show the average spike rate. The gray error bands represent mean \pm SD. Dotted red lines
32 represent the firing rate predicted by the model with the presence of presynaptic lateral inhibition (with
33 LI). Dotted green lines represent the firing rate predicted by the model without the presence of LI. The
34 arrows indicate the stimuli in which the model without LI overestimates the neuronal response. The
35 horizontal gray lines represent stimulation time. Dashed vertical lines signal the beginning of the
36 stimulus. **(a)** The model's fits of the firing rate dynamics for ROF stimuli: ME1-3 and OPTO (see Fig.
37 4). **(b)** The model's fits of the firing rate dynamics for TOF stimuli: LOOM, RECED, LOOM-P, and
38 RECED-P (see Fig. 5). **(c)** The model's fits of the firing rate dynamics for looming stimuli with
39 different dynamics of expansion (see Table 1 and Fig. 7). The angular size, $\theta(t)$, of the looming object
40 is represented by the gray curved line at the bottom of each panel

41 TABLE LEGENDS

42
43
44
45
46
47
48
49
50
51
52
53
54
55
56 **Table 1. Looming stimulus parameters** (see Fig. 1b). Looming stimulus parameters (stimuli 1-6),
57 where l is the half-size of the object, v is the approach speed, L is the initial distance, T is the travel
58
59
60
61
62
63
64
65

1
2
3
4
5
6
7
8
9
10
11
12
13
14
15
16
17
18
19
20
21
22
23
24
25
26
27
28
29
30
31
32
33
34
35
36
37
38
39
40
41
42
43
44
45
46
47
48
49
50
51
52
53
54
55
56
57
58
59
60
61
62
63
64
65

time between the initial position to the collision, and θ is the angular size of the object in degrees. The parameter l/v and θ_0 are used to describe the dynamics in terms of time to collision (see Eq. 1)

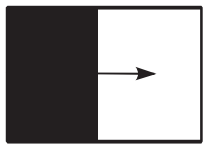
Abbreviations

- LGMD** Lobula Giant Motion Detector
- MSN** Motion-sensitive neuron
- LSN** Looming-sensitive neuron
- DCMD** Descending contralateral movement detector
- MLG** Monostratified lobula giant
- OF** Optical flow
- ROF** Rotational optical flow
- TOF** Translational optical flow
- FFE** Feed-forward Excitation
- FFI** Feed-forward Inhibition
- LI** Lateral Inhibition

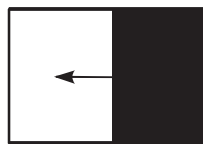
Stimulus Number	l (cm)	v (cm/s)	l/v (ms)	L (m)	T (s)	θ_0 (deg)
1	8.5	142.5	56	5	3.5	1.9
2	17	142.5	120	5	3.5	3.9
3	32	142.5	225	5	3.5	7.3
4	64	142.5	450	5	3.5	14.5
5	17	71.5	238	5	7	3.9
6	17	286	60	5	1.75	3.9

a

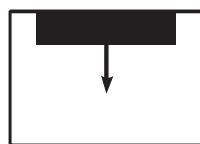
(i) ME-1



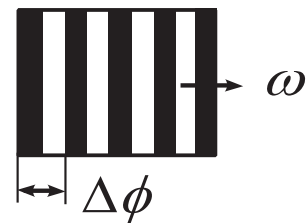
(ii) ME-2



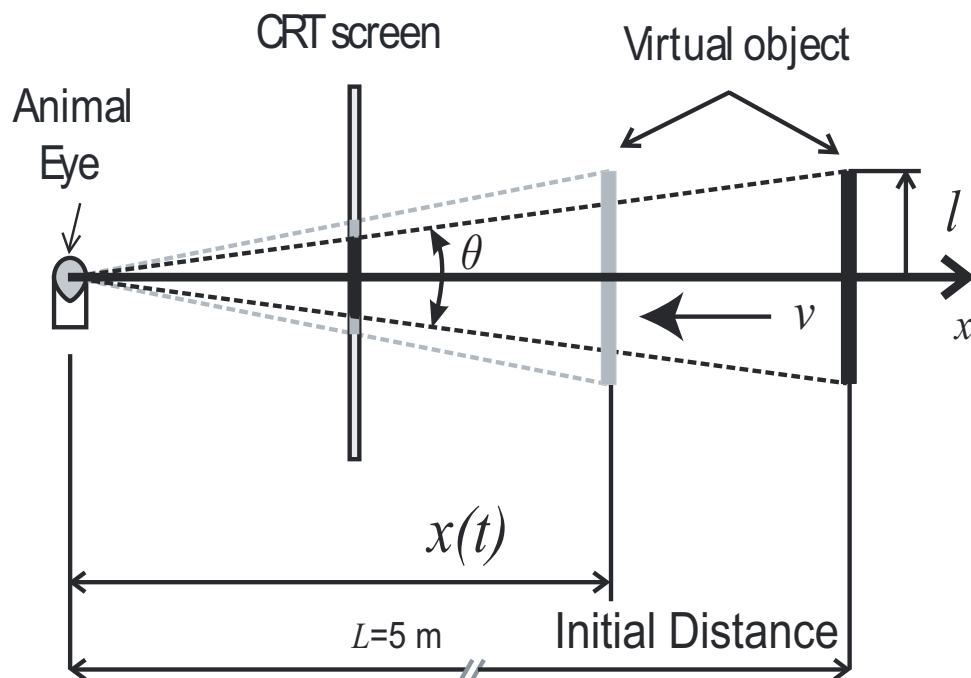
(iii) ME-3



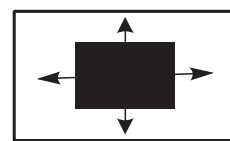
(iv) OPTO



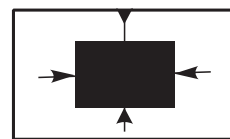
b



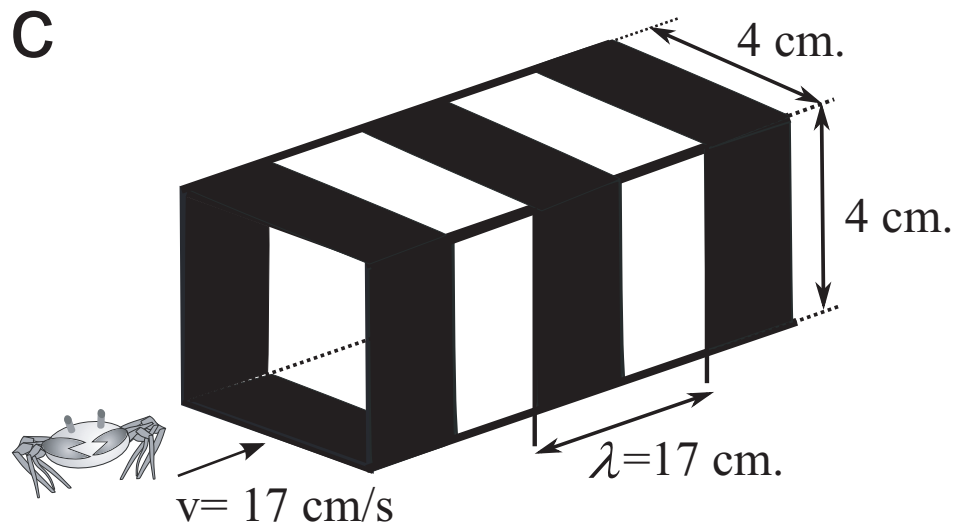
(i) LOOM



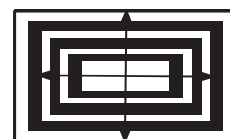
(ii) RECED



c



(i) LOOM-P



(ii) RECED-P

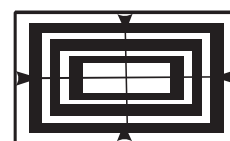


Figure 1

Figure 2

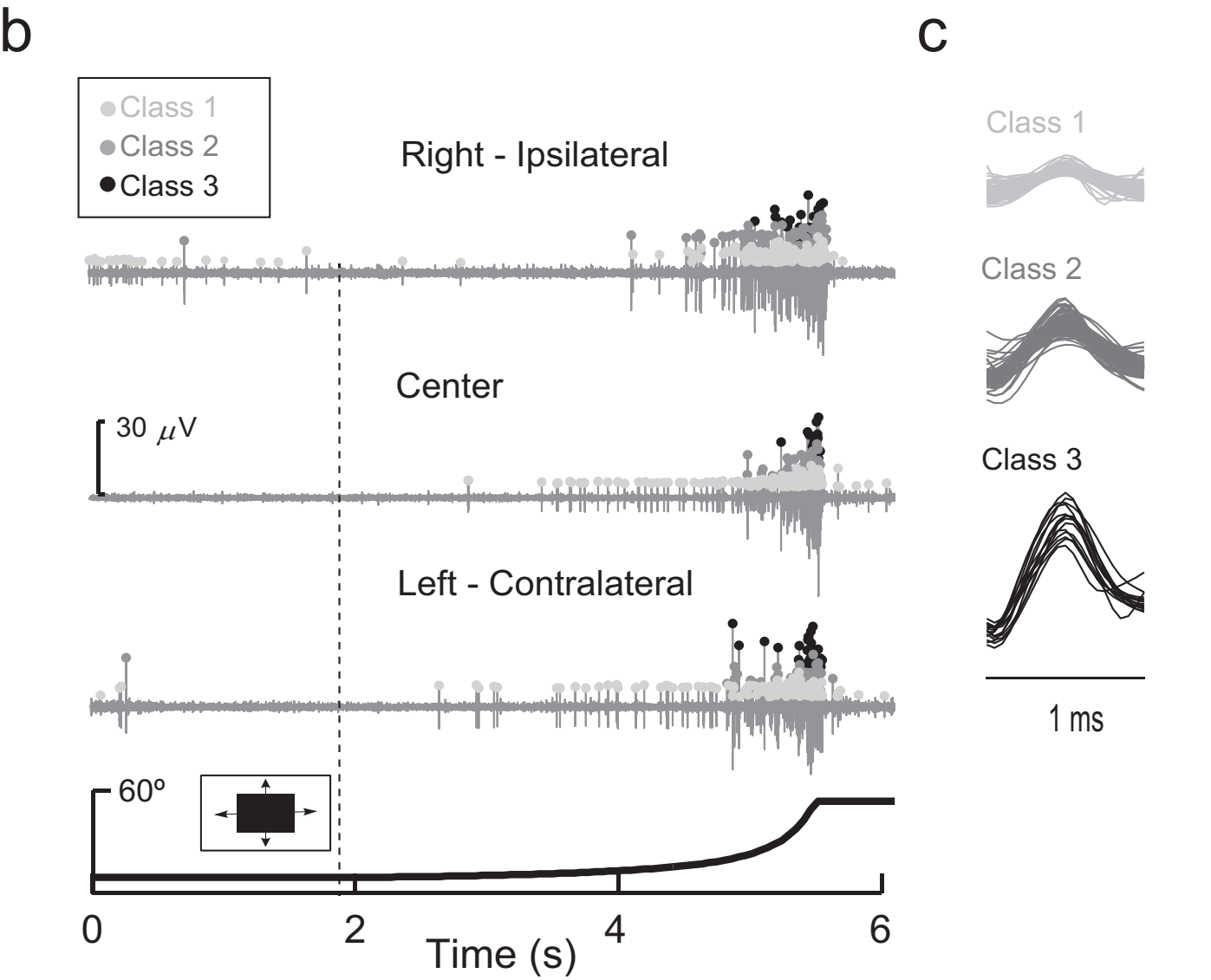
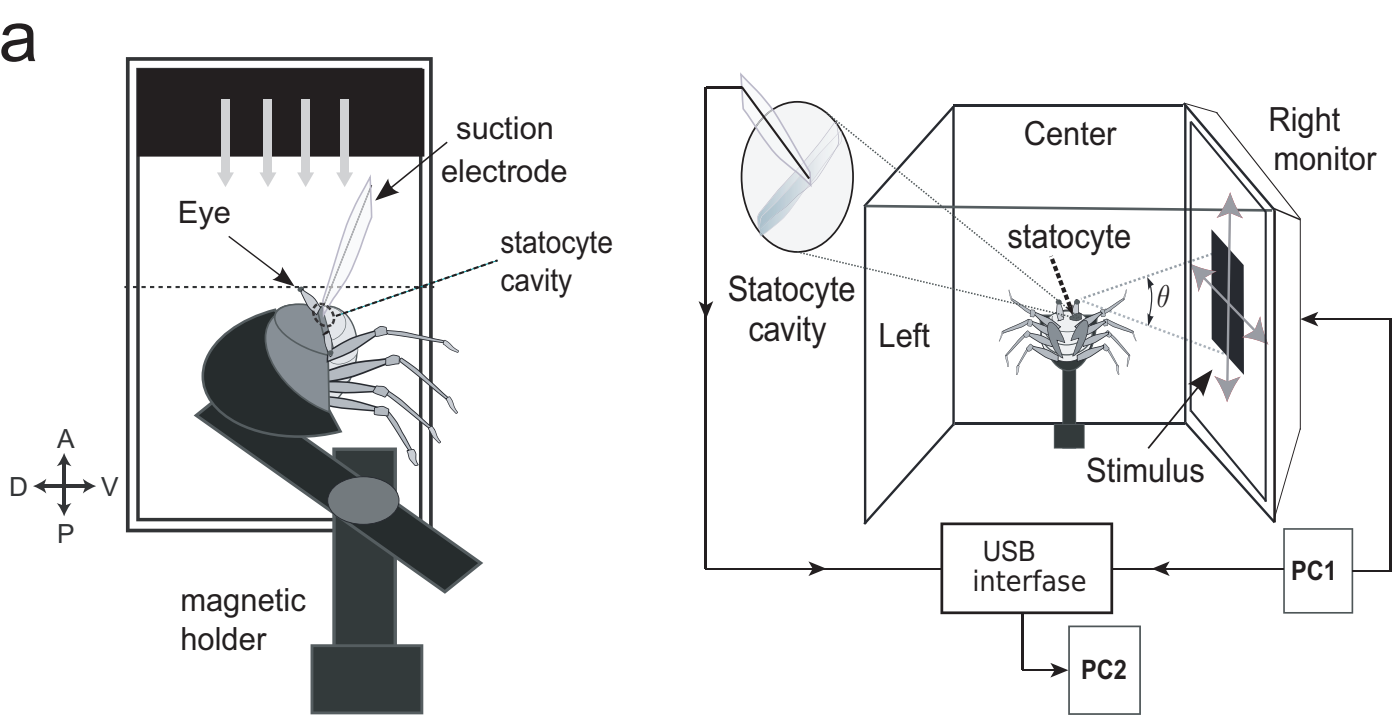


Figure 2

Figure 3

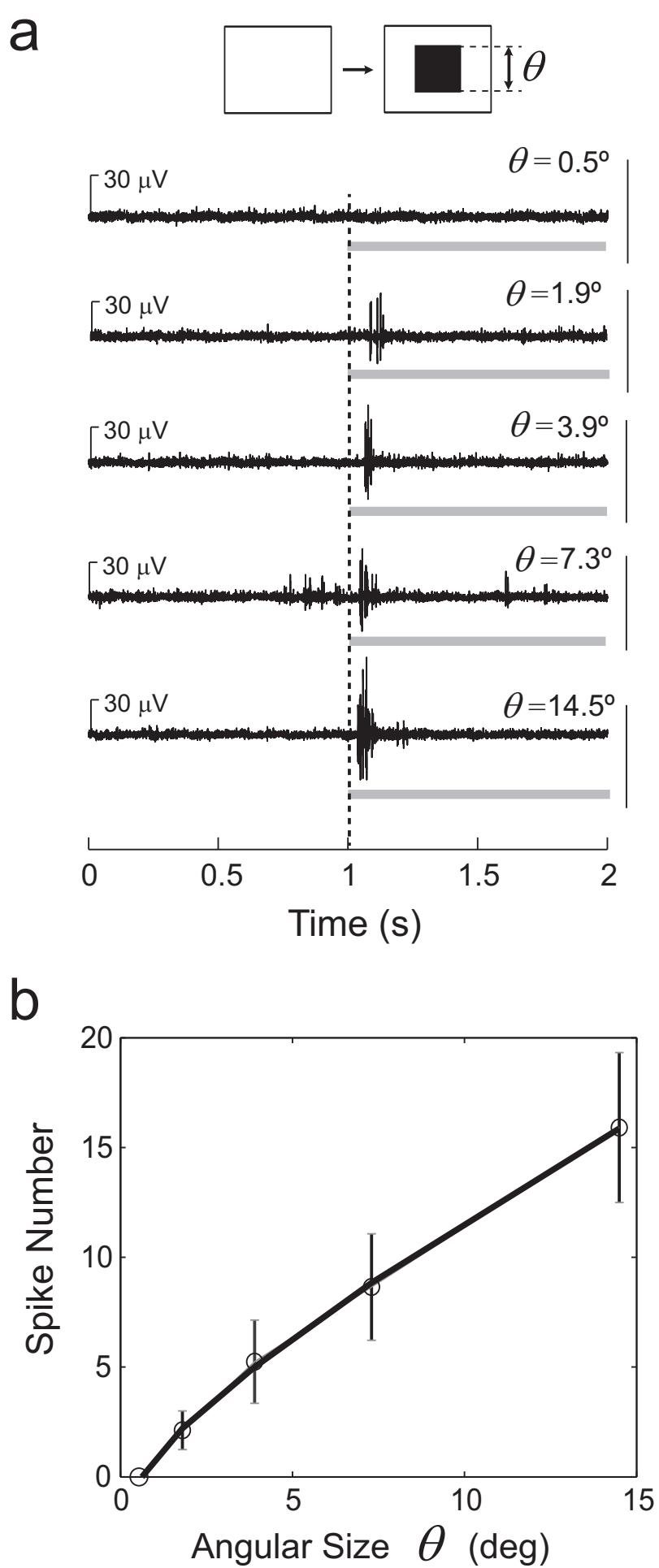


Figure 3

Figure 5

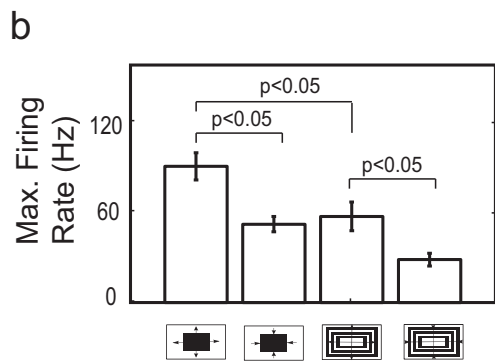
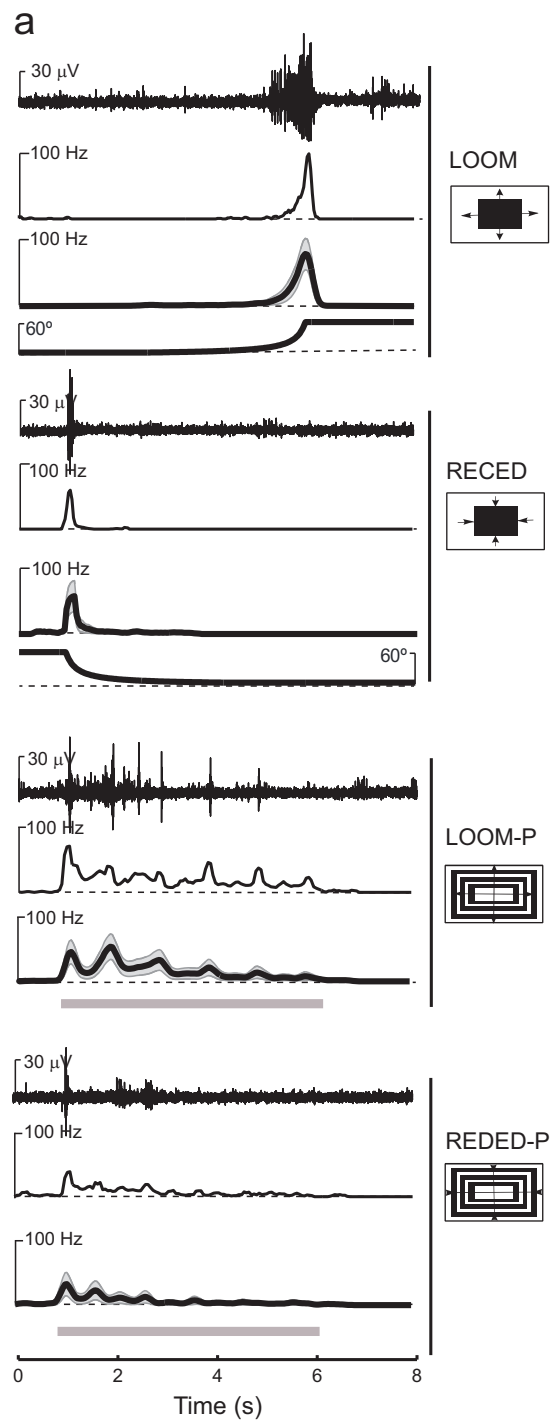
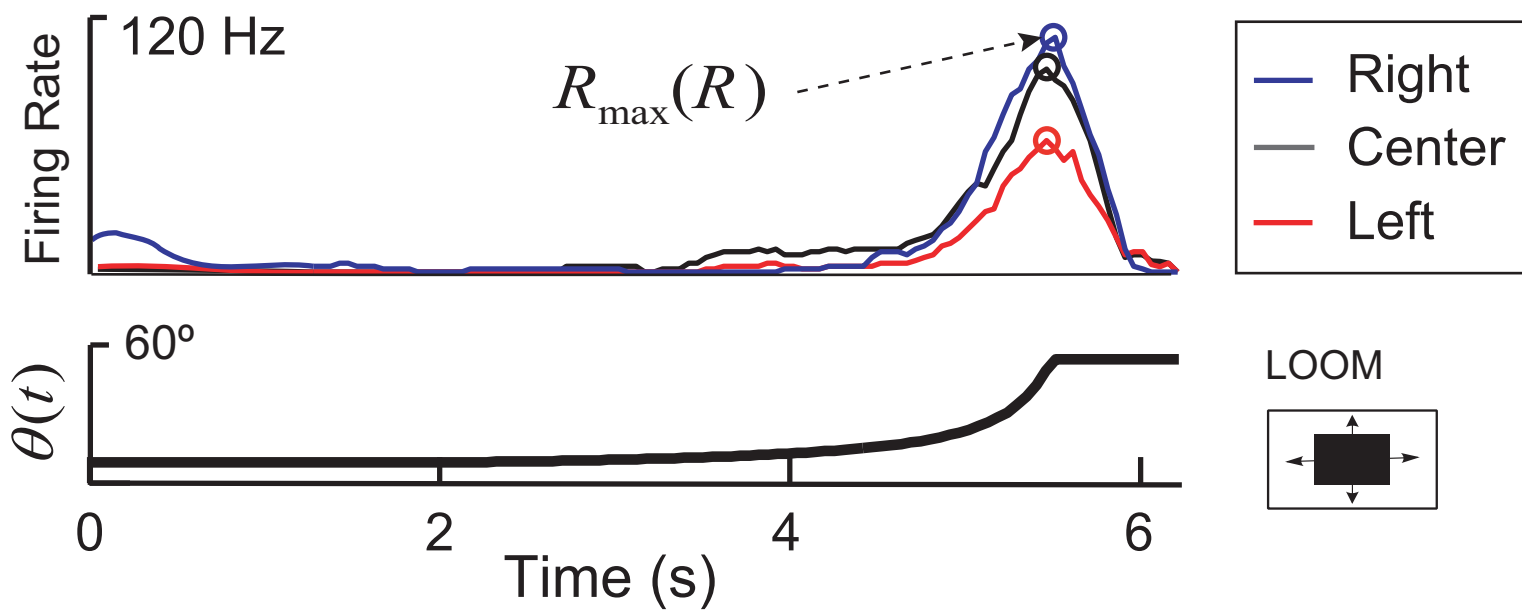


Figure 5

Figure 6

a



b

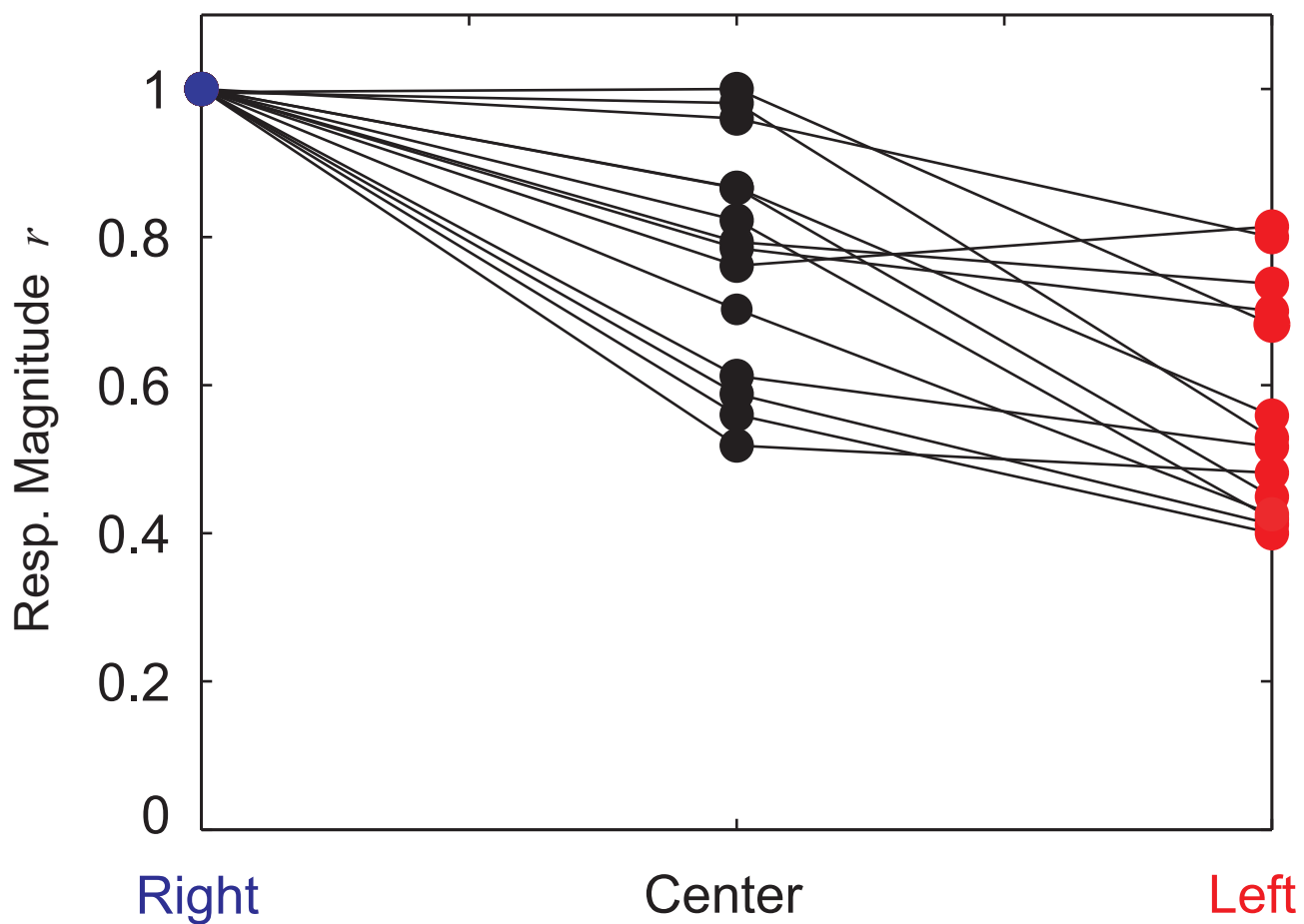


Figure 6

Figure 7

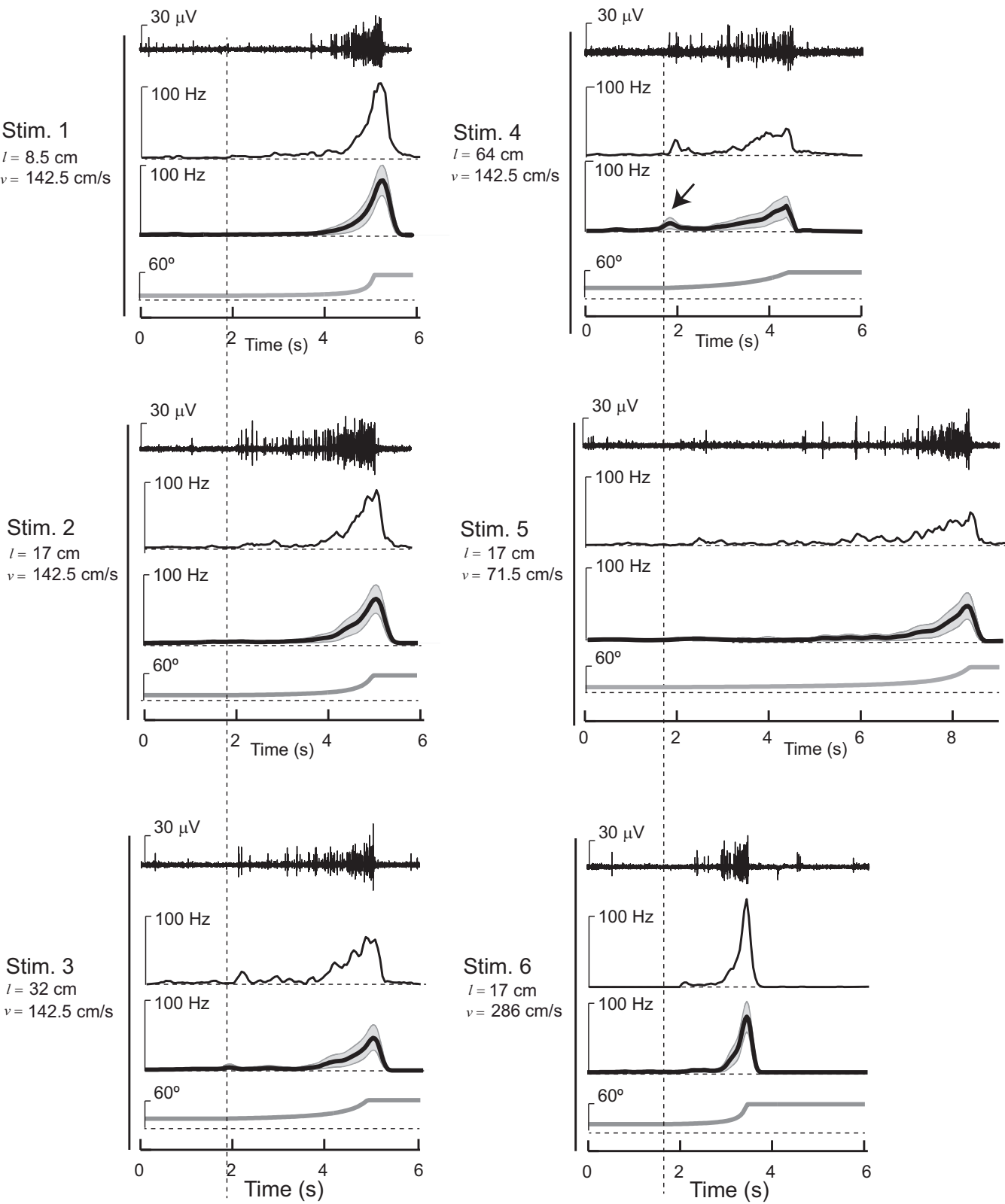


Figure 7

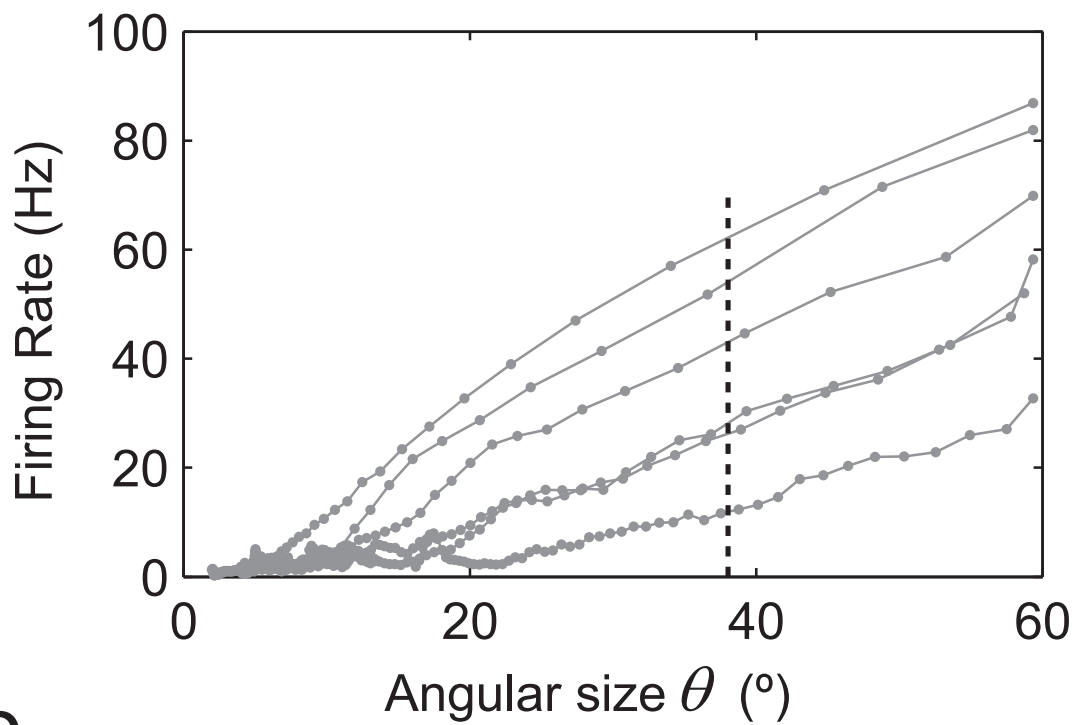
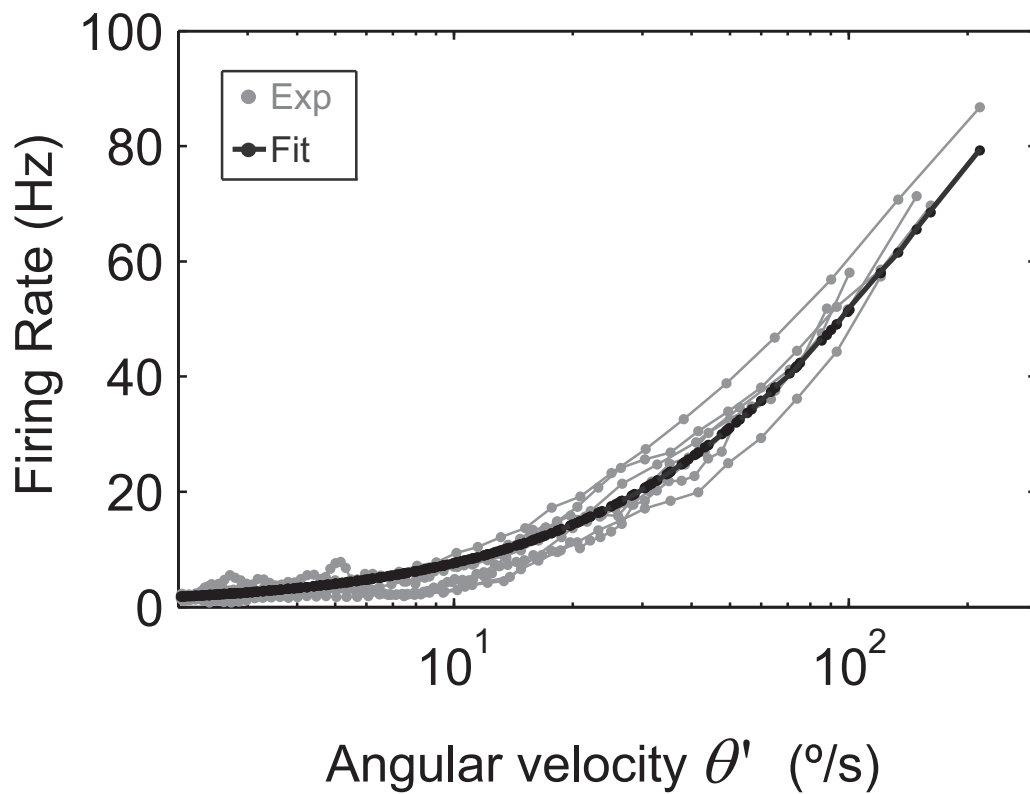
a**b****Figure 8**

Figure 9

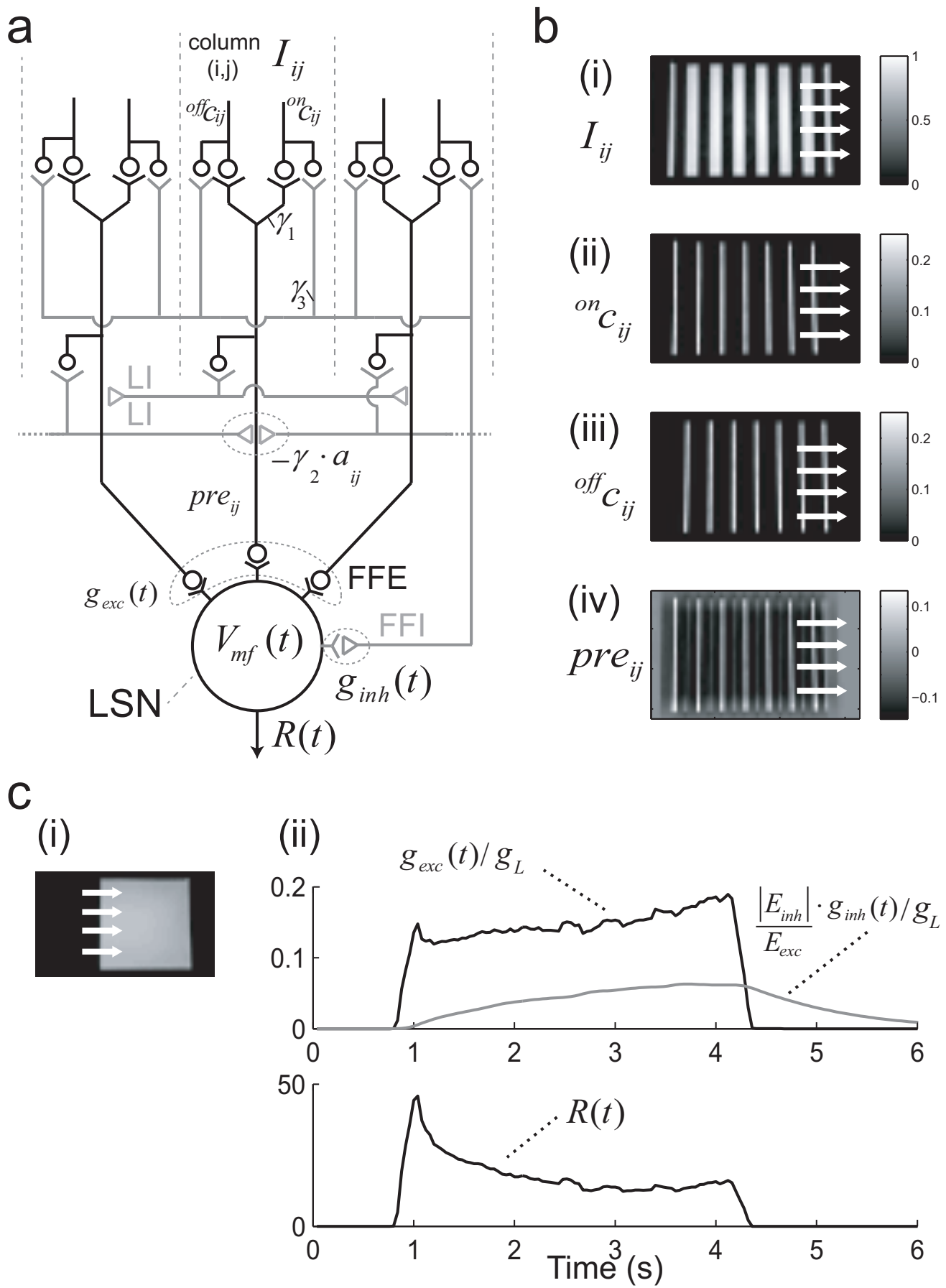


Figure 9

Figure 10

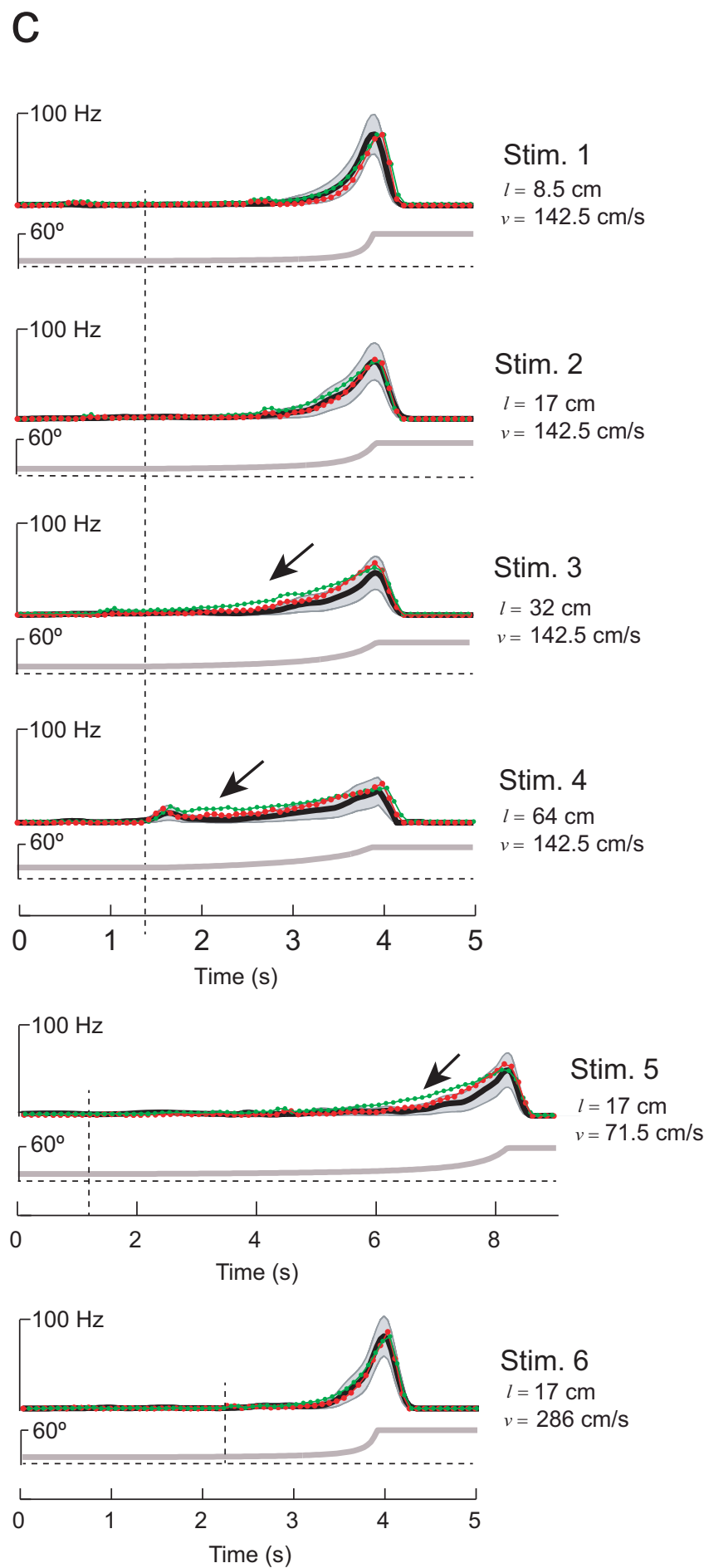
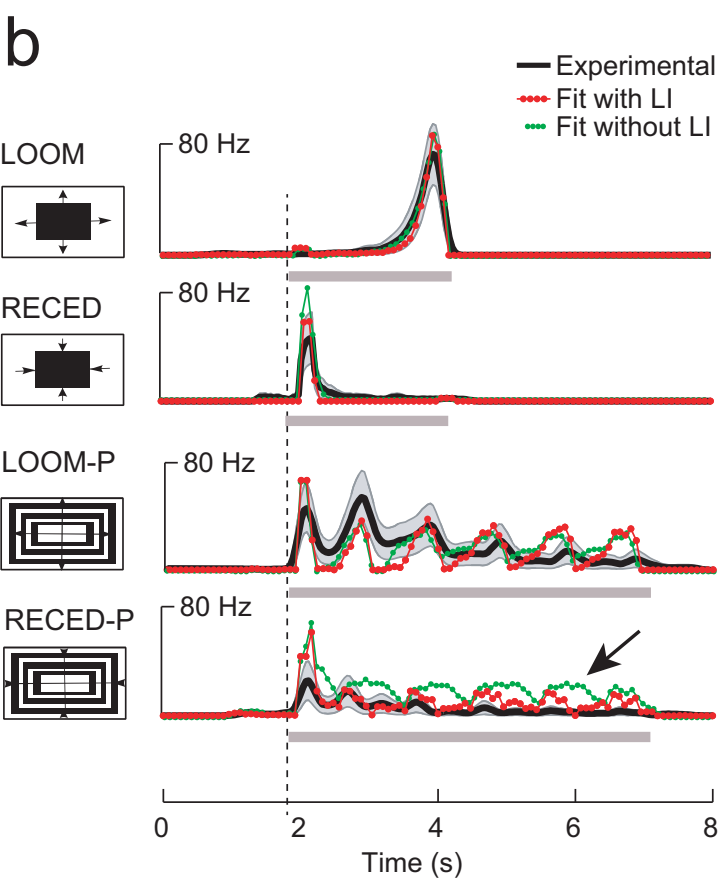
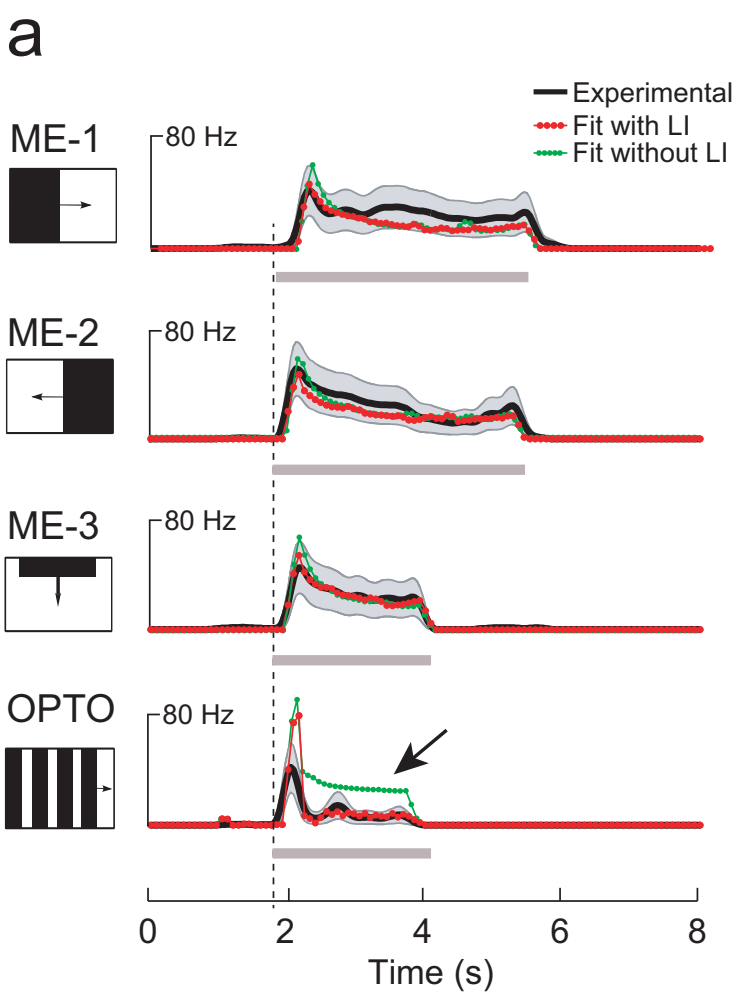


Figure 10